FERMILAB-PUB-12-258-PPD

Neutral B-meson mixing from three-flavor lattice QCD: Determination of the $SU(3)$-breaking ratio ξ

A. Bazavov,[1] C. Bernard,[2] C.M. Bouchard,[3,4,5] C. DeTar,[6] M. Di Pierro,[7] A.X. El-Khadra,[3] R.T. Evans,[3,8] E.D. Freeland,[3,9] E. Gámiz,[4,10,*] Steven Gottlieb,[11] U.M. Heller,[12] J.E. Hetrick,[13] R. Jain,[3] A.S. Kronfeld,[4] J. Laiho,[14] L. Levkova,[6] P.B. Mackenzie,[4] E.T. Neil,[4] M.B. Oktay,[6] J.N. Simone,[4] R. Sugar,[15] D. Toussaint,[16] and R.S. Van de Water[1]

(Fermilab Lattice and MILC Collaborations)

[1] *Physics Department, Brookhaven National Laboratory, Upton, New York, USA*
[2] *Department of Physics, Washington University, St. Louis, Missouri, USA*
[3] *Physics Department, University of Illinois, Urbana, Illinois, USA*
[4] *Fermi National Accelerator Laboratory, Batavia, Illinois, USA*
[5] *Department of Physics, The Ohio State University, Columbus, Ohio, USA*
[6] *Physics Department, University of Utah, Salt Lake City, Utah, USA*
[7] *School of Computing, DePaul University, Chicago, Illinois, USA*
[8] *Department of Nuclear Engineering, North Carolina State University, Raleigh, North Carolina, USA*
[9] *Department of Physics, Benedictine University, Lisle, Illinois, USA*
[10] *CAFPE and Departamento de Física Teórica y del Cosmos, Universidad de Granada, Granada, Spain*
[11] *Department of Physics, Indiana University, Bloomington, Indiana, USA*
[12] *American Physical Society, Ridge, New York, USA*
[13] *Physics Department, University of the Pacific, Stockton, California, USA*
[14] *SUPA, School of Physics and Astronomy, University of Glasgow, Glasgow, Scotland, UK*
[15] *Department of Physics, University of California, Santa Barbara, California, USA*
[16] *Department of Physics, University of Arizona, Tucson, Arizona, USA*

(Dated: March 6, 2013)

Abstract

We study $SU(3)$-breaking effects in the neutral B_d-$\bar{B}_d$ and B_s-$\bar{B}_s$ systems with unquenched $N_f = 2+1$ lattice QCD. We calculate the relevant matrix elements on the MILC collaboration's gauge configurations with asqtad-improved staggered sea quarks. For the valence light-quarks (u, d, and s) we use the asqtad action, while for b quarks we use the Fermilab action. We obtain $\xi = f_{B_s}\sqrt{B_{B_s}}/f_{B_d}\sqrt{B_{B_d}} = 1.268 \pm 0.063$. We also present results for the ratio of bag parameters B_{B_s}/B_{B_d} and the ratio of CKM matrix elements $|V_{td}|/|V_{ts}|$. Although we focus on the calculation of ξ, the strategy and techniques described here will be employed in future extended studies of the B mixing parameters $\Delta M_{d,s}$ and $\Delta\Gamma_{d,s}$ in the Standard Model and beyond.

* megamiz@ugr.es

I. INTRODUCTION

The observation of new particles at high-energy colliders is not the only way for new physics to be discovered. It can also be unveiled through the observation of deviations from the Standard Model (SM) via high-precision measurements of low-energy observables in high-luminosity experiments. This requires matching precision in the theoretical SM predictions for these observables. In principle, such a comparison could reveal the exchange of virtual, new heavy particles involving scales much higher than those that can be achieved in direct production at high-energy colliders.

Heavy-flavor physics and, in particular, neutral-meson mixing are potentially very sensitive to these virtual effects. Neutral-meson mixing occurs at loop level in the SM, see Fig. 1, and it is further suppressed by small Cabibbo–Kobayashi-Maskawa (CKM) matrix elements, so the effect of new particles in the internal loops could be noticeable in the parameters describing the mixing. Indeed, there are several measurements for which there is a 2–3σ difference from the SM prediction. These include $\sin(2\beta)$ [1], the like-sign dimuon charge asymmetry [2], and unitarity triangle (UT) fits [3–7]. It has been argued that these differences may be due to physics beyond the Standard Model (BSM) affecting the neutral B-meson mixing processes [3, 4].

In the B_s^0 system, the relative phase between the decay amplitudes with and without mixing, β_s, could also show BSM effects, as pointed out in Ref. [8] and later hinted at in a Tevatron measurement [9]. Although new measurements at CDF [10] and DØ [11] are in better agreement with the SM, reducing the difference from $\sim 3\sigma$ to $\sim 1\sigma$, there is still room for a large deviation of β_s from SM values.

The main parameters describing mixing in the B_s^0 and the B_d^0 systems are the mass differences, $\Delta M_{s(d)}$, and the decay width differences, $\Delta\Gamma_{s(d)}$, between the heavy and light $B_{s(d)}^0$ mass eigenstates, and the CP violating phases $\phi_{s(d)}$. The phases $\phi_{s(d)}$ are defined as the argument of the ratio of the dispersive and absorptive off-diagonal elements of the time evolution matrix which describes the mixing [12]. The existence of new, heavy particles in loops could affect the value of the mass differences, given by the dispersive part of the time evolution matrix. The mass differences ΔM_s [13–15] and ΔM_d [16] have been measured with an accuracy better than 1%. Improving the theoretical control on these quantities is thus crucial in order to fully exploit the potential of CP violating observables to search for nonstandard physics. In addition, the theoretical calculation of BSM contributions to mixing and the experimental measurement of B^0 mixing parameters can help in constraining BSM parameters and understanding new physics [6]. Several recent studies have addressed that task [3–7, 17–24], finding that one of the main limitations to further constraining the parameter space in BSM theories is the error associated with the theoretical calculation of the nonperturbative inputs.

The most interesting quantity to analyze in B^0 mixing phenomena is the $SU(3)$-breaking ratio ξ, which measures the difference between the mixing parameters in the B_s^0 and the B_d^0 systems, and enters the relation between the ratio of mass differences and CKM matrix elements as

$$\left|\frac{V_{td}}{V_{ts}}\right| = \xi\sqrt{\frac{\Delta M_d M_{B_s}}{\Delta M_s M_{B_d}}}\,. \tag{1.1}$$

Its value, together with the experimental measurement of the mass differences $\Delta M_{s,d}$, determines the ratio of CKM matrix elements $|V_{td}/V_{ts}|$, which constrains one side of the unitarity

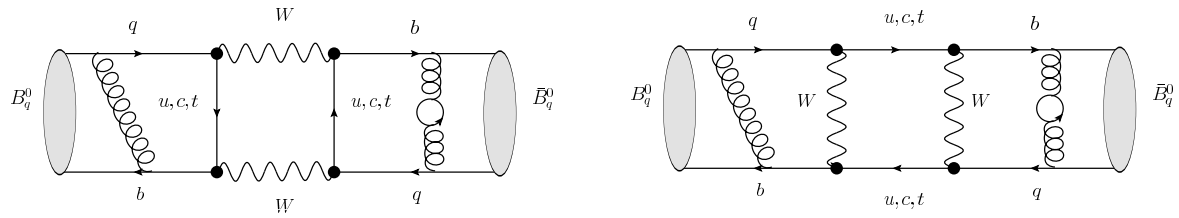

FIG. 1. Box diagrams contributing to $B^0 - \bar{B}^0$ mixing in the SM. Gluon exchanges shown in the plot are just representative of the QCD corrections.

triangle [25, 26]. Thus, ξ is one of the key ingredients in UT analyses [3, 5–7].

In the SM, mixing is due to box diagrams with the exchange of two W-bosons, like those in Fig. 1. These box diagrams can be rewritten in terms of an effective Hamiltonian with four-fermion operators describing processes with $\Delta B = 2$. In BSM theories, mixing processes can receive contributions from additional diagrams due to the exchange of new, heavy particles. These can also be parametrized in terms of four-fermion effective operators built with SM degrees of freedom. The most general effective Hamiltonian describing processes with $\Delta B = 2$ was given in [27, 28], and can also be found in [29]. There are a total of five independent operators (plus parity conjugates) in the Hamiltonian, but only three of them contribute to mixing in the SM

$$\mathcal{H}_{\rm eff,SM}^{\Delta B=2} = \sum_{i=1}^{3} C_i \mathcal{O}_i \,, \tag{1.2}$$

with

$$\begin{aligned} \mathcal{O}_1^q &= \left(\bar{q}^i \gamma^\nu \, L \, b^i\right) \left(\bar{q}^j \gamma^\nu \, L \, b^j\right) \,, \\ \mathcal{O}_2^q &= \left(\bar{q}^i \, L \, b^i\right) \left(\bar{q}^j \, L \, b^j\right) \,, \\ \mathcal{O}_3^q &= \left(\bar{q}^i \, L \, b^j\right) \left(\bar{q}^j \, L \, b^i\right) \,, \end{aligned} \tag{1.3}$$

where i and j are color indices, and L and R are the Dirac projection operators $\frac{1}{2}(1-\gamma_5)$ and $\frac{1}{2}(1+\gamma_5)$ respectively. The fields q denote strange or down fields for B_s^0 and B_d^0 mixing respectively, and b represents the bottom field.

The matrix element of the first operator in Eq. (1.3), $\mathcal{O}_1^q$, provides the mass difference in the SM:

$$\Delta M_q^{SM} = \frac{G_F^2 M_W^2}{6\pi^2} |V_{tq}^* V_{tb}|^2 \eta_2^B S_0(x_t) M_{B_q} f_{B_q}^2 \hat{B}_{B_q} \,, \tag{1.4}$$

where $S_0(x_t)$ is the Inami-Lim function [30], which depends on the top quark mass through $x_t = m_t^2/M_W^2$, and the quantity η_2^B is a perturbative QCD correction factor. The products $f_{B_q}^2 \hat{B}_{B_q}$ parametrize the hadronic matrix elements in the effective theory by

$$\langle \bar{B}_q^0 | \mathcal{O}_1^q | B_q^0 \rangle(\mu) = \frac{2}{3} M_{B_q}^2 f_{B_q}^2 B_{B_q}(\mu) \,. \tag{1.5}$$

The factors f_{B_q} are the B_q^0 decay constants. The renormalization group invariant bag parameters $\hat{B}_{B_q}$ in Eq. (1.4) are related to the scheme and scale dependent bag parameters in

(1.5) at next-to-leading order (NLO) by

$$\hat{B}_{B_q} = [\alpha_s(\mu)]^{-6/23} \left[1 + \frac{\alpha_s(\mu)}{4\pi} J_5\right] B_{B_q}(\mu)\,, \tag{1.6}$$

where J_5 is known in both $\overline{\rm MS}$-NDR (naive dimensional regularization) and $\overline{\rm MS}$-HV ('t Hooft-Veltman) schemes [31]. Bag parameters have traditionally been used to measure the deviation of the four-fermion operator matrix elements from their vacuum insertion values, $B_B = 1$.

The $SU(3)$-breaking parameter ξ can be written in terms of decay constants and bag parameters

$$\xi = \frac{f_{B_s}\sqrt{B_{B_s}}}{f_{B_d}\sqrt{B_{B_d}}}\,. \tag{1.7}$$

Many of the uncertainties that affect the theoretical calculation of the decay constants and bag parameters cancel totally or partially in this ratio, leaving the chiral extrapolation as the dominant error. Hence, ξ and the combination of CKM matrix elements related to it, can be determined with a significantly smaller error than the individual matrix elements.

The hadronic matrix elements in Eq. (1.5) encode the nonperturbative physics of the problem and are best calculated using lattice QCD. Our current knowledge of them limits the accuracy with which the CKM matrix elements appearing in Eq. (1.4) can be determined from the experimental measurements of $\Delta M_{s(d)}$. In particular, the uncertainty associated with the calculation of ξ is one of the main limiting factors in UT analyses, so improvement in the knowledge of ξ is crucial to disentangle the origin of the 2–3σ tension.

There are two $2+1$ unquenched lattice calculations of the ratio ξ in the literature. One is by the HPQCD collaboration [32], which quotes the value $\xi = 1.258(33)$. The other is an exploratory study by the RBC and UKQCD collaborations [33] on a single lattice spacing and using the static limit for the bottom quark; their result is $\xi = 1.13(12)$. In this paper, we report a lattice calculation of ξ at the few percent level.

Preliminary results related to the work here were presented in [34–37]. In Ref. [34], the simulation and correlator fitting methods were described using data for one lattice spacing, while Refs. [35, 36] focused on the discussion of statistical and fitting errors, and the chiral extrapolation method. In Ref. [37] we studied the matching method and the heavy-quark discretization errors.

The primary difference between this work and the HPQCD calculation in Ref. [32] is the treatment of the valence b quarks. The HPQCD collaboration uses lattice NRQCD [38] while we employ the clover action [39] with the Fermilab interpretation [40]. An advantage of the Fermilab method is that it can also be efficiently used to simulate charm quarks, so the analysis performed in this work can be easily extended to the study of the short-distance contributions to D^0-$\bar{D}^0$ mixing. Although in the case of neutral D mixing the long-distance contributions are believed to be dominant, a calculation of the short-distance contributions nevertheless can provide valuable constraints on extensions of the SM [41].

In order to achieve the few-percent level of precision required by phenomenology, we use lattice QCD simulations with realistic sea quarks. In particular, we employ a subset of the MILC configurations with 2+1 flavors of asqtad sea quarks [42–44]. In the valence sector, we use the same staggered asqtad action to simulate the light quarks. The configurations we use in this analysis were generated using the fourth-root procedure for eliminating extra

degrees of freedom originating from fermion doubling. Despite the nonlocal violations of unitarity of the rooted theory at non-zero lattice spacing [45, 46], there are strong theoretical arguments [47–50], as well as other analytical and numerical evidence [51–54], that the local, unitary theory of QCD is recovered in the continuum limit. This gives us confidence that the rooting procedure yields valid results. We also explicitly tested the rooting procedure as well as improvements in our heavy action by calculating the spin-dependent hyperfine splittings for B_s and D_s mesons in Ref. [55].

Our collaboration has already successfully used the asqtad MILC ensembles in similar calculations of other quantities involving B mesons, as part of a broad program of calculating matrix elements: for example, the extraction of the CKM matrix elements $|V_{ub}|$ and $|V_{cb}|$ from the calculation of, respectively, the semileptonic form factors describing the processes $B \to \pi l\nu$ [56] and $B \to D^* l\nu$ [57, 58]; or, more recently, the calculation of the f_B and f_{B_s} decay constants [59] and the form-factor ratios between the semileptonic decays $\bar{B} \to D^+ l^- \bar{\nu}$ and $\bar{B}_s \to D_s^+ l^- \bar{\nu}$ [60].

This paper is organized as follows. In Sec. II, we describe the actions and parameters used in our numerical simulations, as well as the construction of the mixing operators and correlation functions. Section III presents the renormalization method using one-loop mean-field improved lattice perturbation theory. We include a discussion of the errors associated with the matching and numerical values of the matching coefficients used. Next, in Sec. IV, we give the details of the procedure for the correlator fits. Section V is devoted to the chiral-continuum extrapolation, which is performed within the framework of rooted staggered chiral perturbation theory [63–67]. We describe and discuss the choice of the functional form used in the extrapolation, the different fitting methods tested, and the choice of parameters and parametrization. In Sec. VI, we list and estimate the different systematic errors. Finally, Section VII compiles our final results for the parameter ξ as well as for $|V_{td}|/|V_{ts}|$, and the ratio of bag parameters B_{B_s}/B_{B_d}. We also discuss planned future improvements in the calculation of B^0 mixing parameters by our collaboration. In Appendix A, we provide the explicit formulas for the chiral fit functions used in the chiral fits described in Section V. In Appendix B, we compile the functions needed to estimate the heavy-quark discretization errors in our calculation. Finally, Appendix C discusses our choices for prior central values and widths for the correlator fits.

II. NUMERICAL SIMULATIONS

A. Parameters of the simulations

The $n_f = 2 + 1$ MILC ensembles [62] used in our calculation include the effect of three sea-quark flavors: two degenerate light quarks corresponding to the up and down quarks (although with larger masses than the physical ones), and one heavier quark corresponding to the strange quark. These dynamical quarks are simulated using the asqtad improved staggered action with errors starting at $O(\alpha_s a^2)$ [68]. The gluon action is a Symanzik improved and tadpole improved action, with $O(\alpha_s a^2)$ errors coming from the gluon loops removed [69, 70]. The couplings needed to remove the $O(\alpha_s a^2)$ errors coming from quark loops [71] were available only after the generation of configurations was well advanced, so these effects are not accounted for in the MILC ensembles. The dominant errors in the gauge action are thus also of $O(a^4, \alpha_s a^2)$.

The valence light-quark propagators are generated using the asqtad action and converted

TABLE I. Parameters of the ensembles analyzed in this work. The first two rows show the approximate lattice spacing and the volume. am_l and am_h are the light and strange sea quark masses, respectively. $N_{\rm confs}$ is the number of configurations analyzed from each ensemble, and am_q are the light valence quark masses. The r_1/a values are obtained by fitting the calculated r_1/a to a smooth function [61], as explained in Ref. [62].

$\approx a$(fm)	$\left(\frac{L}{a}\right)^3 \times \frac{T}{a}$	am_l/am_h	$N_{\rm confs}$	am_q	r_1/a
0.12	$24^3 \times 64$	0.005/0.05	529	0.005, 0.007, 0.01, 0.02, 0.03, 0.0415	2.64
0.12	$20^3 \times 64$	0.007/0.05	833	0.005, 0.007, 0.01, 0.02, 0.03, 0.0415	2.63
0.12	$20^3 \times 64$	0.01/0.05	592	0.005, 0.007, 0.01, 0.02, 0.03, 0.0415	2.62
0.12	$20^3 \times 64$	0.02/0.05	460	0.005, 0.007, 0.01, 0.02, 0.03, 0.0415	2.65
0.09	$28^3 \times 96$	0.0062/0.031	557	0.0031, 0.0044, 0.062, 0.0124, 0.0272, 0.031	3.70
0.09	$28^3 \times 96$	0.0124/0.031	534	0.0031, 0.0042, 0.062, 0.0124, 0.0272, 0.031	3.72

to naive quark propagators using the relation [72]

$$S_{\rm naive}(x,y) = \Omega(x)\Omega^\dagger(y) S_{\rm staggered}(x,y). \tag{2.1}$$

where $\Omega(x) = \gamma_0^{x_0}\gamma_1^{x_1}\gamma_2^{x_2}\gamma_3^{x_3}$.

For the heavy bottom quarks we use the Sheikholeslami-Wohlert action [39] with the Fermilab interpretation for heavy-quark systems [40]. This interpretation retains the full mass dependence of the theory within the parameters of the lattice action. A tree-level matching to QCD is then performed via heavy quark effective theory (HQET), after which it can be shown that the errors in the action begin at $O(\alpha_s\Lambda_{\rm QCD}a, \Lambda^2_{\rm QCD}a^2)$ times bounded functions of $m_b a$, the b-quark mass in lattice units.

We perform our analysis at two different values of the lattice spacing, $a \approx 0.12, 0.09$ fm, and for a variety of sea-quark masses. The values used are shown in Table I. The mass of the heavy b quark is fixed to its physical value by computing the spin-averaged B_s kinetic mass [55]. This determines the b quark's hopping parameters, $\kappa_b = 0.0860$ for the $a \approx 0.12$ fm lattice and $\kappa_b = 0.0923$ for the $a \approx 0.09$ fm lattice [55], and thus the bare b quark mass. We simulate the B mesons with the six different values of light-valence quark mass listed in Table I, the smallest of which is around $m_s/8$, in order to facilitate the extrapolation/interpolation to the physical down/strange quark masses.

B. Correlators: the open-meson propagator

As described in the introduction, the study of the $SU(3)$-breaking ratio ξ requires the calculation of the hadronic matrix elements[1] $\langle \mathcal{O}_1^q \rangle$ and $\langle \mathcal{O}_2^q \rangle$, the latter of which mixes with $\langle \mathcal{O}_1^q \rangle$ under renormalization, for both $q = d, s$. The matrix elements are obtained from three-point correlation functions with zero spatial momentum

$$C_{\mathcal{O}_i^q}(t_x, t_y) = \sum_{\boldsymbol{x},\boldsymbol{y}} \langle \bar{B}_q^0(t_y, \boldsymbol{y}) \mathcal{O}_i^q(0) B_q^0(t_x, \boldsymbol{x})^\dagger \rangle \,, \tag{2.2}$$

[1] To simplify the notation, we define $\langle \mathcal{O}_i^q \rangle \equiv \langle \bar{B}_q^0 | \mathcal{O}_i^q | B_q^0 \rangle$ for $i = 1, 2$.

where $i = 1$ or 2, and the B-meson creation operator $B_q^0(t,\boldsymbol{x})^\dagger = \sum_{\boldsymbol{x'}} \bar{b}(t,\boldsymbol{x'})S(\boldsymbol{x},\boldsymbol{x'})\gamma_5 q(t,\boldsymbol{x})$, with $q(t,\boldsymbol{x})$ the naive light quark field, whose propagator is constructed from the staggered propagator *via* Eq. (2.1), and with $S(x,x')$ a smearing function. Our choice of smearing function is discussed in Sec. IV A. The structure of the functions in (2.2) is depicted in Fig. 2. The four-fermion operators $\mathcal{O}_i^q$ are placed at the origin while B-mesons are positioned at x and y. This layout allows us to perform the three-point function fits over both t_x and t_y, maximizing the information included in the fits. In order to extract the relevant matrix elements from (2.2), we need to determine the overlap of the B-meson creation operator with the ground state. Therefore, we also need the pseudoscalar two-point correlator with zero spatial momentum

$$C_{PS}(t) = \sum_{\boldsymbol{x}} \langle B_q^0(t,\boldsymbol{x}) B_q^0(0,\boldsymbol{0})^\dagger \rangle \,. \tag{2.3}$$

The calculation of both three-point and two-point correlators can be organized into convenient structures. Starting with a general correlator with Dirac structure $\Gamma_1 \times \Gamma_2$, which accommodates a full set of $\Delta B = 2$ four-quark operators, including those in Eq. (1.3),

$$C_3(t_x,t_y) = \sum_{\boldsymbol{x},\boldsymbol{y}} \langle \bar{B}_q^0(t_y,\boldsymbol{y})\bar{q}(0)\Gamma_1 b(0)\bar{q}(0)\Gamma_2 b(0) B_q^0(t_x,\boldsymbol{x})^\dagger \rangle \,, \tag{2.4}$$

and performing the four possible Wick contractions, we obtain

$$\begin{aligned} C_3(t_x,t_y) = \sum_{\boldsymbol{x},\boldsymbol{y}} \Big\{ & \operatorname{tr}[\gamma_5 L_q(x,0)\Gamma_1 H_b(0,x)] \operatorname{tr}[\gamma_5 L_q(y,0)\Gamma_2 H_b(0,y)] \\ & + \operatorname{tr}[\gamma_5 L_q(y,0)\Gamma_1 H_b(0,y)] \operatorname{tr}[\gamma_5 L_q(x,0)\Gamma_2 H_b(0,x)] \\ & - \operatorname{tr}[\gamma_5 L_q(x,0)\Gamma_1 H_b(0,y)\gamma_5 L_q(y,0)\Gamma_2 H_b(0,x)] \\ & - \operatorname{tr}[\gamma_5 L_q(x,0)\Gamma_2 H_b(0,y)\gamma_5 L_q(y,0)\Gamma_1 H_b(0,x)] \Big\} \qquad (2.5) \\ = \sum_{\boldsymbol{x},\boldsymbol{y}} \Big\{ & \operatorname{tr}[L_q(x,0)\Gamma_1\gamma_5 H_b^\dagger(x,0)] \operatorname{tr}[L_q(y,0)\Gamma_2\gamma_5 H_b^\dagger(y,0)] \\ & + \operatorname{tr}[L_q(y,0)\Gamma_1\gamma_5 H_b^\dagger(y,0)] \operatorname{tr}[L_q(x,0)\Gamma_2\gamma_5 H_b^\dagger(x,0)] \qquad (2.6) \\ & - \operatorname{tr}[L_q(x,0)\Gamma_1\gamma_5 H_b^\dagger(y,0) L_q(y,0)\Gamma_2\gamma_5 H_b^\dagger(x,0)] \\ & - \operatorname{tr}[L_q(x,0)\Gamma_2\gamma_5 H_b^\dagger(y,0) L_q(y,0)\Gamma_1\gamma_5 H_b^\dagger(x,0)] \Big\}, \qquad (2.7) \end{aligned}$$

where L_q is the (naive) light-quark propagator, and H_b is the heavy-quark propagator. The traces in Eq. (2.5) run over spin and color indices.

These correlators can be rewritten as

$$\begin{aligned} C_3(t_x,t_y) = {} & \Gamma_1^{\beta\alpha} E_{aa}^{\alpha\beta}(t_x) \Gamma_2^{\tau\sigma} E_{cc}^{\sigma\tau}(t_y) + \Gamma_1^{\beta\alpha} E_{aa}^{\alpha\beta}(t_y) \Gamma_2^{\tau\sigma} E_{cc}^{\sigma\tau}(t_x) \\ & - \Gamma_1^{\beta\alpha} E_{ac}^{\alpha\sigma}(t_x) \Gamma_2^{\sigma\tau} E_{ca}^{\tau\beta}(t_y) - \Gamma_1^{\beta\alpha} E_{ac}^{\alpha\sigma}(t_y) \Gamma_2^{\sigma\tau} E_{ca}^{\tau\beta}(t_x) \,, \end{aligned} \tag{2.8}$$

where summation over repeated indices is implied, and we have introduced the basic objects

$$E_{ac}^{\alpha\beta}(t) = \gamma_5^{\alpha\sigma} H_{b,da}^{*\tau\sigma}(t,0) L_{q,dc}^{\tau\beta}(t,0) \,, \tag{2.9}$$

with Dirac indices labeled as $\alpha, \beta, \sigma, \tau$ and color indices labeled as a, c, d. We call the combination of propagators $E_{ad}^{\alpha\beta}(t_x)$ defined in Eq. (2.9) "open-meson propagator". Once the

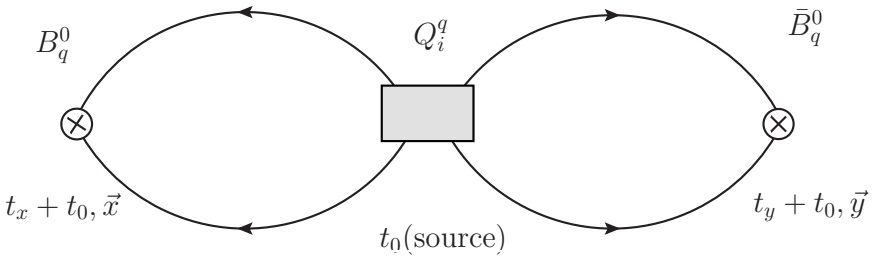

FIG. 2. Structure of the three-point correlators. A B_q^0 is created at rest at $t_x + t_0 < t_0$. At time t_0, it oscillates into a $\bar{B}_q^0$ via the operator $\mathcal{O}_i^q$, which is subsequently annihilated at $t_y + t_0 > t_0$.

open-meson propagators have been computed and saved, all correlation functions needed for B-meson mixing, including BSM operators, can be immediately constructed by contracting them with the appropriate Dirac structures. As shown in Eq. (2.8) the three-point correlators are obtained by combining two open-meson propagators, while for the two-point correlators we only need one open-meson propagator.

C. Doubler modes' effect on the correlation functions

The remnant doubling degeneracy of staggered fermions leads to contributions of scalar states, in addition to pseudoscalar states, in correlation functions with external pseudoscalar particles. The scalar contamination yields oscillating terms in the correlation functions [72]. In this section, we extend the analysis of Ref. [72], for two-point correlation functions, to the three-point functions introduced in Section II B. We conclude that the effect of the doubler modes on the three-point functions can be removed at leading order in the lattice spacing through appropriate fits of the Euclidean time-dependence.

The *doubling* symmetry of the original naive action under the transformation

$$\psi(x) \to e^{ix\cdot\pi_g} M_g \psi(x)\,, \qquad \bar{\psi(x)} \to e^{ix\cdot\pi_g} \bar{\psi}(x) M_g^\dagger\,, \tag{2.10}$$

where

$$M_g = \prod_{\mu\in g} i\gamma_5\gamma_\mu\,, \tag{2.11}$$

$$G = \{g : g = (\mu_1, \mu_2, \ldots), \mu_1 < \mu_2 < \ldots\}, \tag{2.12}$$

$$(\pi_g)_\mu = \begin{cases} \frac{\pi}{a} & \text{if } \mu \in g \\ 0 & \text{otherwise} \end{cases} \tag{2.13}$$

generates sixteen equivalent species of quarks, referred to as *tastes*, that can be reduced to four by staggering the quark field [73]. Each element of G is a list of up to four indices, e.g., (2), (0,3), and (0,1,2,3) are elements of G, as is the empty set $\emptyset$. Different g's label different doubler modes, or tastes.

Consider the general three-point function in momentum space,

$$C_{\Gamma_1\times\Gamma_2}(t_x,t_y) \equiv \sum_{\boldsymbol{x},\boldsymbol{y}} \langle \bar{b}(x)\gamma_5 q(x)\,[\bar{q}(0)\Gamma_1 b(0)\bar{q}(0)\Gamma_2 b(0)]\,\bar{b}(y)\gamma_5 q(y)\rangle = \int_{-\pi/a}^{\pi/a} \frac{d^3\boldsymbol{p}}{(2\pi)^3}\frac{d^3\boldsymbol{k}}{(2\pi)^3} \langle \bar{\tilde{b}}(\boldsymbol{p},t_x)\gamma_5\tilde{q}(\boldsymbol{p},t_x)\,[\bar{q}(0)\Gamma_1 b(0)\bar{q}(0)\Gamma_2 b(0)]\,\bar{\tilde{b}}(\boldsymbol{k},t_y)\gamma_5\tilde{q}(\boldsymbol{k},t_y)\rangle\,, \quad (2.14)$$

where $\Gamma_1\times\Gamma_2$ denotes the Dirac structure of the four-fermion operators in (1.3). For simplicity of notation, we omit the smearing function from the B meson operator and write it as $\bar{b}(x)\gamma_5 q(x)$. It would be straightforward (but not particularly instructive) to generalize the expressions of Eqs. (2.14)–(2.20) to include the smearing function.

For now the bracketed four-quark operator is left in position space and $\tilde{b},\tilde{q}$ are the spatial momentum-space bottom and strange/down fermion fields. Because of the doubling symmetry, we can integrate over the central half of the Brillouin zone and sum over the spatial doublers

$$C_{\Gamma_1\times\Gamma_2}(t_x,t_y) = \sum_{g_s,g_s'} \int_{-\pi/2a}^{\pi/2a} \frac{d^3\boldsymbol{p}}{(2\pi)^3}\frac{d^3\boldsymbol{k}}{(2\pi)^3} \langle \bar{\tilde{b}}(\boldsymbol{p}+\pi_{g_s},t_x)\gamma_5\tilde{q}(\boldsymbol{p}+\pi_{g_s},t_x)\,[\bar{q}(0)\Gamma_1 b(0)\bar{q}(0)\Gamma_2 b(0)]\times \bar{\tilde{b}}(\boldsymbol{k}+\pi_{g_s'},t_y)\gamma_5\tilde{q}(\boldsymbol{k}+\pi_{g_s'},t_y)\rangle, \quad (2.15)$$

where g_s denotes a particular spatial doubler mode. Due to the high momentum that is imparted to the heavy quark when $g_s\neq\emptyset$, such states are far off-shell and have a negligible effect on the correlation function. The taste of the temporal modes can now be considered by Fourier transforming the light quarks' temporal component, and then again restricting the Brillouin zone and summing over the doublers

$$\begin{aligned} C_{\Gamma_1\times\Gamma_2}(t_x,t_y) = \int_{-\pi/2a}^{\pi/2a} \frac{d^3\boldsymbol{p}}{(2\pi)^3}\frac{d^3\boldsymbol{k}}{(2\pi)^3} \int_{-\pi/2a}^{\pi/2a} \frac{dp_0}{(2\pi)}\frac{dk_0}{(2\pi)} e^{ip_0 t_x + ik_0 t_y} \quad (2.16)\\ \times\Big\langle \bar{\tilde{b}}(\boldsymbol{p},t_x)\gamma_5\left[\tilde{q}'(\boldsymbol{p},p_0)+(-1)^{t_x}\tilde{q}'(\boldsymbol{p},p_0+\pi/a)\right]\\ \times[\bar{q}(0)\Gamma_1 b(0)\bar{q}(0)\Gamma_2 b(0)]\,\bar{\tilde{b}}(\boldsymbol{k},t_y)\gamma_5\left[\tilde{q}'(\boldsymbol{k},k_0)+(-1)^{t_y}\tilde{q}'(\boldsymbol{k},k_0+\pi/a)\right]\Big\rangle. \end{aligned}$$

With the momentum space spinors $\tilde{f'}^g$ defined as

$$\tilde{f'}^g(p) = \sum_{\mu\in g} i\gamma_5\gamma_\mu \tilde{q}'(p+\pi_g) \quad (2.17)$$

so that

$$\tilde{q}'(\boldsymbol{p},p_0) = \tilde{f}'(\boldsymbol{p},p_0), \quad \tilde{q}'(\boldsymbol{p},p_0+\pi/a) = i\gamma_5\gamma_0\tilde{f'}^0(\boldsymbol{p},p_0), \quad (2.18)$$

the three-point function can be written as

$$\begin{aligned} C_{\Gamma_1\times\Gamma_2}(t_x,t_y) = \int_{-\pi/2a}^{\pi/2a} \frac{d^3\boldsymbol{p}}{(2\pi)^3}\frac{d^3\boldsymbol{k}}{(2\pi)^3} \Big\langle \bar{\tilde{b}}(\boldsymbol{p},t_x)\gamma_5\left[\tilde{f}(\boldsymbol{p},t_x)+(-1)^{(t_x)}i\gamma_5\gamma_0\tilde{f}^0(\boldsymbol{p},t_x)\right]\\ \times[\bar{q}(0)\Gamma_1 b(0)\bar{q}(0)\Gamma_2 b(0)]\,\bar{\tilde{b}}(\boldsymbol{k},t_y)\gamma_5\left[\tilde{f}(\boldsymbol{k},t_y)+(-1)^{(t_y)}i\gamma_5\gamma_0\tilde{f}^0(\boldsymbol{k},t_y)\right]\Big\rangle, \quad (2.19) \end{aligned}$$

where the superscript 0 indicates a temporal taste and no superscript is the null taste at the center of the Brillouin zone.

After Fourier transforming, the bracketed four-quark operator has no restrictions on the tastes that contribute to it. However, it must be contracted with the external quark fields to form the propagators. Because the asqtad action is used, contractions between tastes of different types are suppressed to $O(a^2\alpha_s^2)$. The three-point function then takes the form

$$\begin{aligned} C_{\Gamma_1\times\Gamma_2}(t_x,t_y) = \int_{-\pi/2a}^{\pi/2a} \frac{d^3\boldsymbol{p}}{(2\pi)^3}\frac{d^3\boldsymbol{k}}{(2\pi)^3} \Big\langle \bar{b}(\boldsymbol{p},t_x)\gamma_5 \left[f(\boldsymbol{p},t_x) + (-1)^{t_x} i\gamma_5\gamma_0 f^0(\boldsymbol{p},t_x)\right] \\ \times \left[\left(\bar{f}(0) + i\gamma_5\gamma_0\bar{f}^0(0)\right)\Gamma_1 b(0)\left(\bar{f}(0) + i\gamma_5\gamma_0\bar{f}^0(0)\right)\Gamma_2 b(0)\right]\bar{b}(\boldsymbol{k},t_y)\gamma_5 \\ \times \left[f(\boldsymbol{k},t_y) + (-1)^{t_y} i\gamma_5\gamma_0 f^0(\boldsymbol{k},t_y)\right]\Big\rangle , \end{aligned} \tag{2.20}$$

where higher order terms coming from contractions between quarks of different taste give terms of $O(a^2\alpha_s^2)$ that are not considered here. The effects of such terms are comparable to NLO terms in staggered chiral perturbation theory and need to be considered at that order. They give rise to the "wrong-spin" terms discussed below. According to Eq. (2.20), the leading-order correlation functions have contributions from both the pseudoscalar and the scalar states. The latter ones are known as oscillating states, since the sign of their contribution oscillates with time.

The fit ansatz for our correlators must model both regular and oscillating contributions, so that we can remove the latter and extract the physical matrix elements. This is done using the form

$$C_{\mathcal{O}_i^q}(t_x,t_y) = \sum_{\alpha,\beta=0}^{N\text{states}-1} Z_\alpha Z_\beta \frac{O^i_{\alpha\beta}}{\sqrt{2E_\alpha 2E_\beta}} (-1)^{(t_x+1)\alpha+(t_y+1)\beta} e^{-E_\alpha t_x - E_\beta t_y} , \tag{2.21}$$

where the sum is over a finite number of states N_{states}. The time t_x in Eq. (2.21) and in the discussion on fitting in Sec. IV is the number of time slices between the initial state and the operator, and thus it is a positive number, unlike the time t_x defined in Fig. 2. The oscillations in Euclidean time given by the factor $(-1)^{(t_x+1)\alpha+(t_y+1)\beta}$ reflect the contribution from the scalar states in Eq. (2.20). The matrix elements of interest are given by the three-point amplitude of the ground state $\alpha = \beta = 0$, O^i_{00}. Analogously, we incorporate regular and oscillating contributions to the description of the two-point correlators by using the following functional form in the fits

$$C_{PS}(t) = \sum_{\alpha=0}^{N_{\text{states}}-1} |Z_\alpha|^2 (-1)^{(t+1)\alpha} \left(e^{-E_\alpha t} + e^{-E_\alpha (T-t)}\right) , \tag{2.22}$$

where T is the temporal size of the lattice. Three- and two-point functions are fit simultaneously in our analysis, as described in Sec. IV.

D. Improving the heavy-light four-quark operator

In addition to the discretization errors in the heavy-quark action, the mixing operator also has discretization errors due to the difference in the small-momentum behavior of lattice

and continuum heavy quarks. In this section, we describe how the lowest order of operator discretization errors are removed in our calculation. We first show that the errors start at $O(a\boldsymbol{p})$ and then discuss how the error at this order can be removed by a "rotation" of the heavy-quark field.

To begin, consider the small $a\boldsymbol{p}$ expansion of the spinor for the Wilson-like fermion

$$\begin{aligned} u^{\rm lat}(\chi,\boldsymbol{p}) &= \frac{\gamma_0 \,{\rm sign}\,\chi \sinh Ea - i\gamma_j \sin(p_j a) + L}{\sqrt{2L(L+\sinh Ea)}} u(\chi,0) \\ &= e^{-m_1 a/2}\left[1 - \frac{i\boldsymbol{\gamma}\cdot\boldsymbol{p}a}{2\sinh m_1 a} + O((a\boldsymbol{p})^2)\right] u(\chi,0), \end{aligned} \tag{2.23}$$

where χ labels spin and particle *vs.* antiparticle, $\hat{p} = (2/a)\sin(pa/2)$, and for the clover action $L = 1 + m_0 a + \frac{1}{2}\hat{\boldsymbol{p}}^2 a^2 - \cos p_0 a$. The continuum spinor has the expansion

$$u^{\rm cont}(\chi,\boldsymbol{p}) = \left[1 - \frac{i\boldsymbol{\gamma}\cdot\boldsymbol{p}}{2m} + O((a\boldsymbol{p})^2)\right] u(\chi,0). \tag{2.24}$$

The mismatch between the small-momentum terms can be easily removed by "rotating" the lattice heavy quark as was done to heavy-light bilinear operators in Ref. [40]. The light lattice spinors for the staggered formulation have the same small-momentum behavior as in the continuum up to $O((\boldsymbol{p}a)^2, (m_q a)^2)$ and need not be matched.

The analysis of Ref. [40] can be generalized from bilinears to four-fermion operators with Dirac structure $\Gamma_1 \times \Gamma_2$. We can take one of the terms in the contraction of the lattice operator

$$\begin{aligned} &\langle q(p'_q), b(p'_b)|\bar{q}\Gamma_1 b \bar{q}\Gamma_2 b|q(p_q), b(p_b)\rangle_{\rm lat} = \\ &N_q(p'_q)N_q(p_q)N_b(p'_b)N_b(p_b)\bar{u}(p'_q)\Gamma_1 u_h^{\rm lat}(p'_b)\bar{u}(p_q)\Gamma_2 u_h^{lat}(p_b) + (\text{additional contractions}), \end{aligned} \tag{2.25}$$

where $N_q(p)$ and $N_b(p)$ are normalization factors for the q and b one-particle states. Following the Fermilab interpretation in Ref. [40], we demand that lattice and continuum amplitudes match through $O(a\boldsymbol{p})$,

$$\begin{aligned} &\mathcal{Z}\left(\bar{u}(\chi,\boldsymbol{p}'_q)\Gamma_1 e^{-am_1^b/2}\left[1 - \frac{i\boldsymbol{\gamma}\cdot\boldsymbol{p}'_b a}{2\sinh am_1^b}\right] u(\chi,0)\right. \\ &\quad \left.\times \bar{u}(\chi,\boldsymbol{p}_q)\Gamma_2 e^{-am_1^b/2}\left[1 - \frac{i\boldsymbol{\gamma}\cdot\boldsymbol{p}_b a}{2\sinh am_1^b}\right] u(\chi,0)\right) + a\mathcal{Z}D_n Q_n \\ &= \bar{u}(\chi,\boldsymbol{p}'_q)\Gamma_1\left[1 - \frac{i\boldsymbol{\gamma}\cdot\boldsymbol{p}'_b}{2m_b}\right] u(\chi,0) \times \bar{u}(\chi,\boldsymbol{p}_q)\Gamma_2\left[1 - \frac{i\boldsymbol{\gamma}\cdot\boldsymbol{p}_b}{2m_b}\right] u(\chi,0) \\ &\quad + O((\boldsymbol{p}a)^2)\,, \end{aligned} \tag{2.26}$$

where Q_n are dimension-seven lattice operators and D_n their corresponding coefficients. These operators and coefficients are straightforward to identify (m_b must be identified with the Fermilab kinetic mass, M_2 [74]). There are two dimension seven operators contributing to the matching, $Q_1 = \bar{q}\Gamma_1 \boldsymbol{\gamma}\cdot\boldsymbol{D} b \bar{q}\Gamma_2 b$ and $Q_2 = \bar{q}\Gamma_1 b \bar{q}\Gamma_2 \boldsymbol{\gamma}\cdot\boldsymbol{D} b$, which will remove the $\boldsymbol{p}a$ discrepancy for appropriate values of the Wilson coefficients and the normalization constant.

From the relation above, we find

$$D_1 = D_2 = \left[\frac{1}{\sinh am_1^b} - \frac{1}{2am_2^b}\right] \tag{2.27}$$

and

$$\mathcal{Z} = e^{am_1^b}. \tag{2.28}$$

Here, m_1 and m_2 are again the Fermilab rest and kinetic masses defined in [40].

However, through $O(a\boldsymbol{p})$, adding these operators has the same effect as inducing a "rotation" of the heavy field

$$b^r(x) = [1 + ad_1\boldsymbol{\gamma}\cdot\boldsymbol{D}]b(x) \tag{2.29}$$

where

$$d_1 = D_1 = D_2. \tag{2.30}$$

This removes $O(\Lambda_{\rm QCD}a)$ discretization errors in the operator. The leading errors are then $O\left((\Lambda_{\rm QCD}a)^2\right)$ and $O(\alpha_s\Lambda_{\rm QCD}a)$. In the way we have set up the calculation, the open-meson propagators, Eq. (2.9), include the rotation.

III. MATCHING OF THE LATTICE MATRIX ELEMENTS

In order to cancel the scheme and scale dependence of the Wilson coefficients in the effective Hamiltonian, we must relate the bare hadronic matrix elements of the lattice operators in Eq. (1.3) to a continuum scheme. We perform that renormalization and matching perturbatively at one loop. In the lattice part of this renormalization calculation we use mean-field improved lattice perturbation theory [75] to improve the convergence of the theory by resumming the tadpole contributions.

Already at one loop, even in the continuum, the operators in Eq. (1.3) mix with each other under renormalization. To extract the renormalized value of $\langle\mathcal{O}_1^q\rangle$, we use the following matching relation

$$\begin{aligned}\langle\mathcal{O}_1^q\rangle^{\rm renor}(\mu) =& \mathcal{C}\,\left\{[1+\alpha_s\cdot\zeta_{11}(\mu,m_b,am_b)]\langle\mathcal{O}_1^q\rangle^{\rm lat} + \alpha_s\cdot\zeta_{12}(\mu,m_b,am_b)\langle\mathcal{O}_2^q\rangle^{\rm lat}\right\}\\ &+O\left(\alpha_s^2,\alpha_s\Lambda_{\rm QCD}a\right)\,,\end{aligned} \tag{3.1}$$

where the renormalization coefficients ζ_{ij} are the difference between the renormalizations in the continuum and on the lattice, $\zeta_{ij} = Z_{ij}^{\rm cont} - Z_{ij}^{\rm lat}$. The continuum renormalization scale at which we perform the matching is μ. The lattice spacing is a and $\mathcal{C}$ is a factor which absorbs the lattice field normalization conventions. The values of $Z_{ij}^{\rm cont}$ are listed in Ref. [76] and a detailed description of the calculation of the lattice renormalization coefficients will be given in Ref. [77]. Table II lists the tadpole-improved renormalization coefficients relevant for the lattice data analyzed in this paper. For each lattice spacing and b quark mass we show the infrared (IR) finite part of the $Z_{ij}^{\rm lat}$'s as well as the corresponding ζ_{ij} (in the $\overline{\rm MS}$-NDR continuum scheme). The ζ_{ij} are IR finite since the IR divergent contributions to $Z_{ij}^{\rm lat}$ and $Z_{ij}^{\rm cont}$ cancel in the difference. All the coefficients $Z_{ij}^{\rm lat}$ in Table II are between 0.3 and 1, which indicates a sensible behavior of the lattice perturbation series.

In order to apply the matching relation Eq. (3.1), we need to choose both a scale μ and a value for the strong coupling constant α_s. For the scale, we use the bottom quark mass and, in that way, eliminate higher-order logarithmic contributions that come in powers

TABLE II. Values of the finite part of the lattice one-loop renormalization coefficients $Z_{ij}^{\rm lat}$, the difference of the continuum and lattice one-loop coefficients ζ_{ij} needed in (3.1) for the 0.12 fm and 0.09 fm lattices, and the coupling α_s used in the matching relation. The continuum ($\overline{\rm MS}$-NDR) scale used in the matching is $\mu = m_b$.

$\approx a$ (fm)	am_b	$Z_{11}^{\rm lat,\,finite}$	$Z_{12}^{\rm lat,\,finite}$	$\zeta_{11}^{\overline{\rm MS}-{\rm NDR}}$	$\zeta_{12}^{\overline{MS}-NDR}$	α_s
0.12	2.1881	-0.726	-0.325	0.1998	-0.312	0.32
0.09	1.7728	-0.945	-0.369	0.3041	-0.268	0.26

of $\log(\mu/m_b)$. For the strong coupling constant, we use the renormalized coupling in the V-scheme [70] evaluated at a scale q^*, as in Ref. [78]. The scale q^* should be the size of a typical gluon loop momentum in this process and can be calculated using the methods outlined in Refs. [70, 79]. Here, we use $q^* = 2/a$ which is close to the calculated value for heavy-light currents using the same actions we are employing [70, 80]. This is justified since the contributions coming from the current renormalization are larger than the intrinsic four-quark contributions [77]. The values of α_V are determined from the static-quark potential in a manner similar to that described in Ref. [78] and are also given in Table II.

IV. FITTING METHOD AND STATISTICAL ERRORS

The correlation functions are calculated at four different time sources t, and then averaged over time sources. For the $a \approx 0.12$ fm ensembles, $t_0 = 0, 16, 32, 48$, and for the $a \approx 0.09$ fm ensembles, $t_0 = 0, 24, 48, 72$. The statistical errors in the data and fits decrease with each additional time source by approximately what is expected, suggesting that the correlators from different time sources are weakly correlated and statistical power is gained by averaging.

In order to extract the renormalized matrix elements, we tried two methods for the correlator fits. In the first method, we fit the bare correlators and combine the results afterwards with the matching coefficients in Sec. III to get the renormalized matrix elements. In the second method, we first apply the matching coefficients to the correlators for each configuration and then perform the fits to obtain the renormalized matrix elements. The central values are nearly identical with both methods, but the errors are slightly better and the fits more stable with the latter, so for the rest of this article we discuss only the results obtained with the second method.

A. Description of the Fitting Method and Stability Tests

The heavy-quark in the two-point and three-point correlation functions is always rotated at the source as explained in Sec. II D. For three-point functions, we smear the heavy quarks at the sink using a function based on the quarkonium 1S wavefunction [81, 82]. For two-point functions, at the sink we either rotate local heavy quarks, or we smear them with a 1S wavefunction. Smearing greatly improves the overlap with the ground state. The additional rotation at the sink is to ensure that the local-local meson correlator is positive-definite. The naive light-quark propagator is always local at source and sink.

The two-point and three-point correlators used to determine the matrix element $\langle \mathcal{O}_1^q \rangle$ on a particular ensemble and for a particular choice of valence-mass m_q are fit simultaneously

using the Bayesian fitting approach described in Refs. [83, 84]. For the matrix elements on the coarse ensembles, we find the smallest errors and greatest stability using three correlators (two two-point correlation functions and one three-point correlation function):

- C_{PS} in Eq. (2.22) with local source and local sink.

- C_{PS} with local source and 1S smeared sink.

- $C_{\mathcal{O}_1^q}$ in Eq. (2.21) with local source and 1S smeared sink.

For the fine ensembles the best results are obtained with only one two point function and one three-point function:

- C_{PS} with 1S smeared source and 1S smeared sink.

- $C_{\mathcal{O}_1^q}$ with local source and 1S smeared sink.

The prior central values function as the initial starting guesses for our fits. Hence we choose ground-state values guided by our data to help the fits converge. The prior central values for the ground-state masses are obtained from effective mass plots. For the overlap factors Z_0^d and Z_0^{1S}, where superscripts d and $1S$ denote factors corresponding to local or 1S smeared sources/sinks, we examine the amplitude of the B meson propagator with the exponential of the ground state removed. We do the same for O_{00}, where the Z_0^{1S} amplitudes are accounted for. The prior widths are taken to be large compared with the statistical error of the parameters as reported by the fitter to avoid influencing our fit results by our choice of priors. For the higher states' overlap factors, the prior width is chosen based on the expectation that the overlaps should not be larger than the corresponding ground state ones. The energy differences have prior central values and widths that allow them to vary from $\Delta E_{i+1,i} \equiv a(E_{i+1} - E_i) \approx 0.14 - 0.37$, where experimental values [16] have been used as a guide. We checked that the prior widths for all fitting parameters are large enough so they do not influence the central value of relevant quantities extracted from the fits.

The same priors are used for all ensembles, except for the masses of the regular and oscillating ground states, E_0 and E_0' respectively. These parameters are strongly determined by the data, and very different at each lattice spacing, therefore the prior choice must also be lattice-spacing dependent. Appendix C contains a list of the prior central values and widths we use in the calculation.

Statistical errors are estimated with the bootstrap method. Specifically, for each ensemble and valence mass, 500 bootstrap ensembles are constructed from the original ensemble by sampling with replacement. A fit is then performed to each ensemble. We find that, as long as the bootstrap ensembles are larger than ~ 100, the estimated error is independent of bootstrap ensemble size. For fitting methodology checks and plotting purposes in Figs. 3–6, statistical errors in the parameters are estimated by the average 68% bootstrap error, which is defined as half of the distance between the two points at which 16% of the distribution has a higher (lower) value.

Autocorrelations necessarily exist between correlation functions calculated on different configurations within an ensemble and can be minimized by binning the data. The autocorrelations are observable only in a few ensemble and valence masses. In many ensembles and mass combinations, the noise is large enough that the autocorrelations are not observable. We choose a conservative bin size of 4.

TABLE III. Number of states and time ranges used for each correlator in the fits for both the $a \approx 0.12$ fm and $a \approx 0.09$ fm ensembles. For the number of states, the first value indicates the number of regular states and the second one the number of oscillating states. The labels between parentheses in the first column indicate the type of source/sink in that correlator.

Correlator	Number of States	Time Range
C_{PS} (local/local)	3+3	2–20
C_{PS} (local/1S)	3+3	2–20
$C_{Q_q^i}$ (local/1S)	2+2	$(2-10)\times(2-10)$

The number of states included in the sum in Eq. (2.21) and the time ranges we use in the fits are shown in Table III. The minimum time slice is fixed to be the same for all the correlators in the fit, three-point as well as two-point. However, the maximum time is fixed separately for the two- and three-point functions. Following Ref. [83], the number of states are determined by first performing the fit using 1+1 states (1 regular state + 1 oscillatory state) starting at large time slices, where the higher energy states no longer contribute significantly and a good χ^2 per degree of freedom (d.o.f.) is obtained (≈ 1). The fit is then performed using one lower time slice as the starting time $t_{\rm min}$, and this is repeated, reducing $t_{\rm min}$ until the χ^2/d.o.f. is no longer reasonable, $\gtrsim 1.5$. Then an additional pair of states is added to the model function, and the process iterated. Once the timeslice $t = 2$ can be included, that number of states is used in our central-value fits.[2]

For the three-point function, we fit using $N_{\rm states} = N_{\rm states}^{\rm regular} + N_{\rm states}^{\rm oscillating} = 2 + 2 = 4$ and timeslices $t_x, t_y \in [2, 10]$ for all ensembles. The two-point functions are fit for $t \in [2, 20]$ using $3 + 3$ states. The output of these fits successfully describe the oscillations in the correlation functions as can be seen in Fig. 3, which shows the typical behavior in one of the ensembles analyzed.

In order to check that this number of states is sufficient, we add more states and examine the stability of the fits. Stability plots over numbers of states for the $a \approx 0.09$ fm ensembles, which illustrate the typical behavior of our fits, are shown in Fig. 4. The stability of central values and errors is very good for $N_{\rm states} \geq 4$ in all cases.

V. CHIRAL PERTURBATION THEORY

The light sea- and valence-quark masses that are used in our lattice simulations have unphysically large values, with our lightest pion mass ≈ 240 MeV. To obtain information about the quark-mass dependence of the relevant matrix elements, which allows us to extrapolate our results to the physical masses, we perform our calculation at six sea $\times$ six valence quark masses, thus including numerous partially quenched data points. In addition, the leading-order taste violations, which arise at $O(a^2\alpha_s)$, are included in the theory and then removed when the extrapolation is performed using rooted heavy-meson staggered chiral perturbation theory (rHMSχPT) [63, 64, 67]. The χPT expression for $\langle \mathcal{O}_1^q \rangle$, as well as for the matrix elements of all the other operators in the $\Delta B = 2$ effective Hamiltonian was first described in Ref. [85] for partially quenched Wilson-type quarks in the framework of

[2] Time slices $t = 0$ and $t = 1$ contain unconstrained contamination from higher energy states. At $t = 0$ all states contribute because they have the same exponential weighting, and $t = 1$ is contaminated by higher energy states because the degrees of freedom of staggered fermions spread over two time slices.

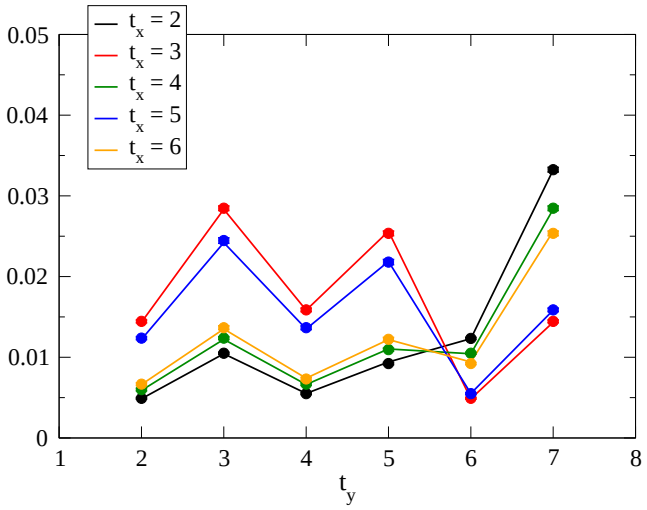

FIG. 3. Comparison of a fit with correlator data for the correlation function $C_{\mathcal{O}_1^q}(t_x, t_y)$ at fixed t_x = 2-6 (labeled by color) and as a function of t_y, for the $a \approx 0.09$ fm ensemble with quark masses 0.0124/0.031 and valence quark mass $am_q = 0.031$. The lines connect the fit function results for integer values of t_x, t_y coming from the same single fit and evaluated at specific t_x, and the dots are the average over simulation data. Statistical errors on the simulation data are smaller than the plot symbols. The fit results describe very well the oscillation in time shown by the data.

continuum heavy-meson χPT (HMχPT). With staggered fermions, we also must include the effects of taste-violating interactions, using rHMSχPT [67].

With the four-quark operators, a careful examination of the Fierz properties shows that there are additional operators with both wrong taste and *spin*, *i.e*, wrong (Γ_1, Γ_2). As far as we know, this property of local heavy-staggered four-quark operators has not been discussed in the literature before. The needed rHMSχPT expressions are derived in Ref. [86]. We became aware of these contributions after our analysis was nearly complete, so we have not included them in the chiral fit functions used here. We do, however, estimate the associated systematic error on ξ in our error budget (cf. Sec. VI C). Explicit expressions for the chiral fit functions used in this work are given in Appendix A.

The NLO rHMSχPT in Eq. (A1) and subsequent equations in the appendix can be schematically written as

$$\begin{aligned} \left\langle \bar{B}_q | \mathcal{O}_1^q | B_q \right\rangle &= \frac{2}{3} M_{B_q}^2 f_{B_q}^2 B_q = \\ & M_{B_q} \alpha \left[1 + (\mathcal{W}_q + \mathcal{T}_q + \mathcal{Q}_q) + L_v m_q + L_s (2m_l + m_h) + L_a a^2 \right] , \end{aligned} \tag{5.1}$$

where α, L_v, L_s, and L_a are low-energy constants (LECs) to be determined from fitting the data, the factor of M_{B_q} comes from the HQET normalization of states, and the masses m_q, m_l, and m_h are the light valence, light sea, and strange sea-quark masses, respectively. The light sea quarks are treated as degenerate, and the isospin average is used, *i.e.*, $\hat{m} = (m_u + m_d)/2$. For staggered quarks the taste-nonsinglet pseudoscalar meson masses are split

$$M_{ij,\rho}^2 = \mu(m_i + m_j) + a^2 \Delta_\rho \,, \tag{5.2}$$

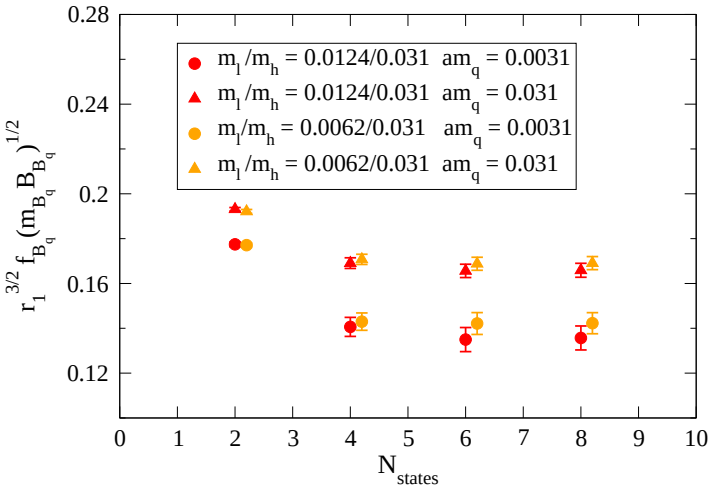

FIG. 4. $r_1^{3/2} f_{B_q} \sqrt{M_{B_q} B_{B_q}}$ for the two $a \approx 0.09$ fm ensembles for $am_q = 0.031, 0.0031$ as a function of the number of states N_{states}. The fit results for $f_{B_q} \sqrt{M_{B_q} B_{B_q}}$ reach a plateau for $N_{\text{states}} \geq 4$.

where m_i and m_j are the quark masses and the sixteen meson masses are labeled by their taste representation, $\rho = P, A, T, V, I$. The parameters μ and the Δ_ρ's are determined from lattice calculations for pions and kaons [87]. Their values are collected in Table IV.

The chiral logarithms, $\mathcal{W}_q$, $\mathcal{T}_q$, $\mathcal{Q}_q$, stem from wavefunction renormalization, tadpole, and sunset diagrams, respectively. The explicit expressions can be found in Appendix A.

In this work, we do not include the effects of the hyperfine splitting Δ^* or the light flavor splittings δ_k defined in the Appendix. The wrong-spin terms contribute to the tadpole and sunset diagrams [86].

When extrapolating to the physical point, we set the parameters Δ_ρ and $\delta'_{A,V}$ (which describe discretization effects) and the lattice spacing to zero, and set the sea quark masses to their physical values, $m_l \to (m_u + m_d)/2$, and $m_h \to m_s$. We then obtain $\langle \bar{B}_d^0 | \mathcal{O}_1^d | B_d^0 \rangle$ or $\langle \bar{B}_s^0 | \mathcal{O}_1^s | B_s^0 \rangle$ by setting $m_q = m_d$ or m_s. Thus, it is an extrapolation to the u- and d-quark masses and an interpolation to the s-quark mass.

An additional consideration is that $SU(3)$ NLO χPT may not be valid for data with masses as large as the strange quark's. It would be desirable to include NNLO contributions to test the validity of the NLO expression, but the effort needed to calculate the NNLO logs is prohibitive. It is reasonable instead to test the chiral expansion by including just NNLO analytic contributions. Wherever the quark masses or splittings are large enough for such analytic NNLO terms to be significant, the NNLO logarithms should be slowly varying and well approximated by the analytic terms. We follow this strategy and supplement the NLO rHMSχPT expressions with NNLO analytic terms in our fits, with prior constraints estimated based on χPT power counting as explained in the next section.

A. Parametrization of the Chiral Expression

Dimensionful quantities are extracted first in units of the lattice spacing and then converted to their physical values using the r_1 scale [88, 89]. This absolute scale is defined

as $r_1^2 F(r_1) = 1.0$, where $F(r_1)$ is the force between static quarks. In our chiral fits, all parameters are first converted to units of r_1 by multiplying by the relative scale r_1/a. The values for r_1/a on every MILC ensemble used in our calculation are listed in Table I. After the chiral-continuum extrapolation, we convert from r_1 units with a physical value of r_1. We take the result obtained by combining the 2009 MILC determination of $r_1 f_\pi$ [90] and the PDG value of f_π [16]. Following Ref. [59], the error for r_1 is determined by averaging the MILC value with the HPQCD value in [91] and then by inflating the uncertainty to take conservatively into account the possible correlations coming from the use of the same configurations in both determinations. The final value we use is $r_1 = 0.3117(22)$ [59]. The error associated with r_1 has a very small effect on the dimensionless quantity ξ.

The dominant lattice artifacts to take into account in our rHMSχPT expressions are expected to be taste violating contributions of $O(a^2\alpha_s^2)$, since the $O(a^2\alpha_s)$ taste-violating effects are absent for asqtad quarks. We parametrize these effects in our fits by defining a quantity A_a^2, which is the ratio of the size of taste violations on lattices with spacing a to those on the $a \approx 0.12$ fm lattices. Thus $A^2_{0.12\,\mathrm{fm}} = 1$ and

$$A^2_{0.09\ \mathrm{fm}} \equiv \frac{(\alpha_s^2 a^2)_{0.09\ \mathrm{fm}}}{(\alpha_s^2 a^2)_{0.12\ \mathrm{fm}}} \sim 0.35\,. \tag{5.3}$$

The NLO rHMSχPT function in Eq. (5.1) can then be rewritten as

$$\begin{aligned}\beta_q \equiv & \sqrt{\frac{3}{2}\langle \bar{B}_q|\mathcal{O}_1^q|B_q\rangle / M_{B_q}} = f_{B_q}\sqrt{M_{B_q}B_{B_q}} \\ & = \beta^\chi\left[1 + \frac{1}{2}(\mathcal{Q}_q + \mathcal{W}_q + \mathcal{T}_q) + \frac{L_v}{2}M_{qq}^2 + \frac{L_s}{2}(2M_{ll}^2 + M_{hh}^2) + \frac{L_a}{2}A_a^2\right], \end{aligned} \tag{5.4}$$

where $\beta^\chi = \sqrt{\alpha}$. The masses M_{ij} are defined in Eq. (5.2), but here we disregard a^2 corrections in the masses since they can be absorbed by a redefinition of the low energy constants at higher order in the chiral expansion. To the NLO expression above we add, inside the square brackets, the allowed NNLO analytic terms, which contribute with seven more unknown LECs

$$\begin{aligned} & Q_1 M_{qq}^4 + Q_2(2M_{ll}^2 + M_{hh}^2)^2 + Q_3 M_{qq}^2(2M_{ll}^2 + M_{hh}^2) \\ & + Q_4(2M_{ll}^4 + M_{hh}^4) + P_1 A_a^2 M_{qq}^2 + P_2 A_a^2(2M_{ll}^2 + M_{hh}^2) + P_3 A_a^4\,. \end{aligned} \tag{5.5}$$

In the above expressions, we have suppressed the factors of r_1 for simplicity. They can be deduced using dimensional considerations. In these expressions, which are the ones we use as fit functions, we write the analytic terms for convenience as functions of the pseudoscalar masses M_{ij} rather than the quark masses.

The ratio ξ can be extracted by first interpolating β_q to $m_q = m_s$ and extrapolating to $m_q = m_d$ separately according to expressions (5.4) and (5.5), and then forming the ratio β_s/β_d. Alternatively, one can consider the ratio of chiral expressions and expand up to

TABLE IV. Inputs for the priors of the free parameters and for the fixed parameters in the fits. The NLO low energy constants L_v, L_s, and L_a are not constrained in the fits. The parameter s is given by the quantity $1/(8\pi^2(r_1 f_\pi)^2)$. We do not consider errors on the slope μr_1 or the taste splittings $r_1^2 a^2 \Delta_\rho$ because those have negligible effect on the final results. In the right hand side table, the two last columns correspond to lattice spacings $a \approx 0.12$ fm and $a \approx 0.09$ fm. See the text for explanations of the choices of parameters.

Fit parameters (central value±width)		
	$a \approx 0.12$ fm	($a \approx 0.09$ fm)
β	1 ± 1	
$g_{B^* B\pi}$	0.51 ± 0.20	
$r_1^2 a^2 \delta'_V$	0.0 ± 0.07	$(0.0 \pm 0.07) \times 0.35$
$r_1^2 a^2 \delta'_A$	-0.28 ± 0.06	$(-0.28 \pm 0.06) \times 0.35$
L_v	unconstrained	
L_s	unconstrained	
L_a	unconstrained	
Q_{1-4}	$0 \pm s^2$	
P_{1-3}	$0 \pm s^2$	

Input (fixed) parameters		
	$a \approx 0.12$ fm	$a \approx 0.09$ fm
$f_\pi r_1$	0.2106	
μr_1	6.234	6.382
$r_1^2 a^2 \Delta_P$	0	0
$r_1^2 a^2 \Delta_V$	0.439	0.152
$r_1^2 a^2 \Delta_T$	0.327	0.115
$r_1^2 a^2 \Delta_A$	0.205	0.0706
$r_1^2 a^2 \Delta_I$	0.537	0.206

NNLO to obtain

$$\xi' = \frac{\beta_{q'}}{\beta_q} = \xi \frac{\sqrt{M_{B_{q'}}}}{\sqrt{M_{B_q}}} = 1 + \frac{1}{2}(\mathcal{Q}_{q'} + \mathcal{W}_{q'} + \mathcal{T}_{q'} - \mathcal{Q}_q - \mathcal{W}_q - \mathcal{T}_q) + \frac{L_v}{2}(M^2_{q'q'} - M^2_{qq}) + Q_1(M^4_{q'q'} - M^4_{qq}) + Q_3(M^2_{q'q'} - M^2_{qq})(2M^2_{ll} + M^2_{hh}) + P_1(M^2_{q'q'} - M^2_{qq})A_a^2 \,, \tag{5.6}$$

with $m_{q'}$ fixed to the value closest to m_s. In Eq. (5.6) we disregard the NNLO terms coming from squaring the NLO terms in the denominator, since they are not necessary to obtain good fits and they are difficult to disentangle from those already included. We can then interpolate/extrapolate to $m_{q'} = m_s$ and $m_q = m_d$. We call these two strategies for the chiral and continuum extrapolation of ξ the indirect and direct methods, respectively. Many of the fit parameters cancel in the chiral expression for ξ' in Eq. (5.6), improving the reliability and stability of the fits. In addition, discretization errors of $O(\alpha_s \Lambda_{\rm QCD} a, (\Lambda_{\rm QCD} a)^2)$ from the heavy-quark action that are not included in the chiral perturbation theory, partially cancel in the ratio. We thus choose this method as our preferred fitting strategy.

B. Results from the chiral fits

In order to perform the chiral fits, we first create 200 bootstrap samples of β_q for each sea- and valence-quark mass combination from the two- and three-point correlator fits. The bootstrap data is then fit to the chiral expression using Bayesian techniques. The fits are simultaneously performed to all ensembles in Table I.

The input and fit parameters are set as in Table IV. We do not impose any constraint on the NLO low energy constants. For the NNLO LECs we use prior widths based on a simple

TABLE V. Results from the rHMSχPT fits. Errors are only statistical and obtained from 200 bootstrap samples. For a full discussion of systematic errors, see Sec. VI.

Ansatz	χ^2/d.o.f.	ξ Direct	χ^2/d.o.f.	ξ Indirect
NNLO	0.45	$1.268^{+0.035}_{-0.044}$	0.23	$1.255^{+0.034}_{-0.041}$
NLO	0.78	$1.284^{+0.018}_{-0.016}$	0.49	$1.262^{+0.008}_{-0.012}$

power counting argument. The NLO analytic terms should be of magnitude similar to the NLO logs, which are $\sim m_\pi^2/(8\pi^2 f_\pi^2) = s(r_1 m_\pi)^2$, (with $s \equiv 1/(8\pi^2(r_1 f_\pi)^2)$). Hence, the NNLO terms are $\sim (m_\pi^2/(8\pi^2 f_\pi^2))^2 = s^2(r_1 m_\pi)^4$. The taste-violating hairpin parameters, δ'_V and δ'_A, were also determined from lattice calculations for pions and kaons in Ref. [62]. We constrain the parameters δ'_V and δ'_A in our fits using the results of Ref. [62] as prior central values and widths. We also take the effective coupling of the $B^*B\pi$ interaction, $g_{B^*B\pi}$, as a fit parameter in our analysis. The prior central value and width we use for this parameter, shown in Table IV, covers the main ranges of determinations of $g_{B^*B\pi}$ [92–98], as discussed in Ref. [57]. A more recent, precise value of $g_{B^*B\pi}$, obtained with $N_f = 2+1$ domain wall fermions and static b quarks [99], was not yet available when this stage of the analysis was carried out. Nevertheless, the result obtained by the authors in Ref. [99], $0.449 \pm 0.047 \pm 0.019$, falls well within the prior central value and width considered here. For the pion decay constant, we use the PDG value, $f_\pi = (130.41 \pm 0.20)$ MeV [16].

The fit results for ξ using different ansatzes for the fitting function and the direct and indirect methods explained in Sec. V A are listed in Table V. The results and errors obtained using the direct and indirect methods agree very well, especially when NNLO terms are included. This constitutes a good check of how well our results are encompassing higher-order terms in the chiral expansion, which are different in these two methods.

In Figs. 5 and 6, we show the NLO and NNLO fit results for ξ from the direct method as a function of the light valence mass in r_1 units, $r_1 m_q$. The top plots in both figures show only the full QCD points, $m_q = m_l$, while the bottom plots show all (partially quenched) data included in the fits (see Table I). The fit curve is the same in both plots of each figure. The black lines show the results of the fit in the continuum limit, after the dominant lattice artifacts are removed using rHMSχPT, and after interpolating the physical sea and valence strange-quark masses to the physical value, as a function of the valence light-quark mass. The black point is our result for ξ at the physical masses, and includes statistical errors.

From the spread of data in the bottom plots of both figures (same data), one can see that the light sea-quark mass dependence is mild; all different sea-quark masses (squares or triangles at a particular axis value) agree within one statistical σ. The discretization errors are also small, as can be seen in both the data and the extrapolation lines in the upper plots.

We obtain fits that match the data well and have good χ^2/d.o.f. with only the inclusion of NLO terms, as shown in Fig. 5. When we add the NNLO terms, the central values for ξ are also within one statistical σ, although errors are significantly larger. This is to be expected, since the NNLO LECs are poorly known. Related to this is the fact that the χ^2/d.o.f. for the NLO fits are larger than for the NNLO fits. At NNLO, we are including extra degrees of freedom with large prior widths that are poorly determined by the fit, so, in practice, we are dividing the same χ^2 by a larger number of degrees of freedom. In fact, the NNLO fits seem to give a slightly better description of the data, as can be seen in the full QCD plots. The chiral extrapolation for ξ is also milder in the NNLO case. Based on these arguments

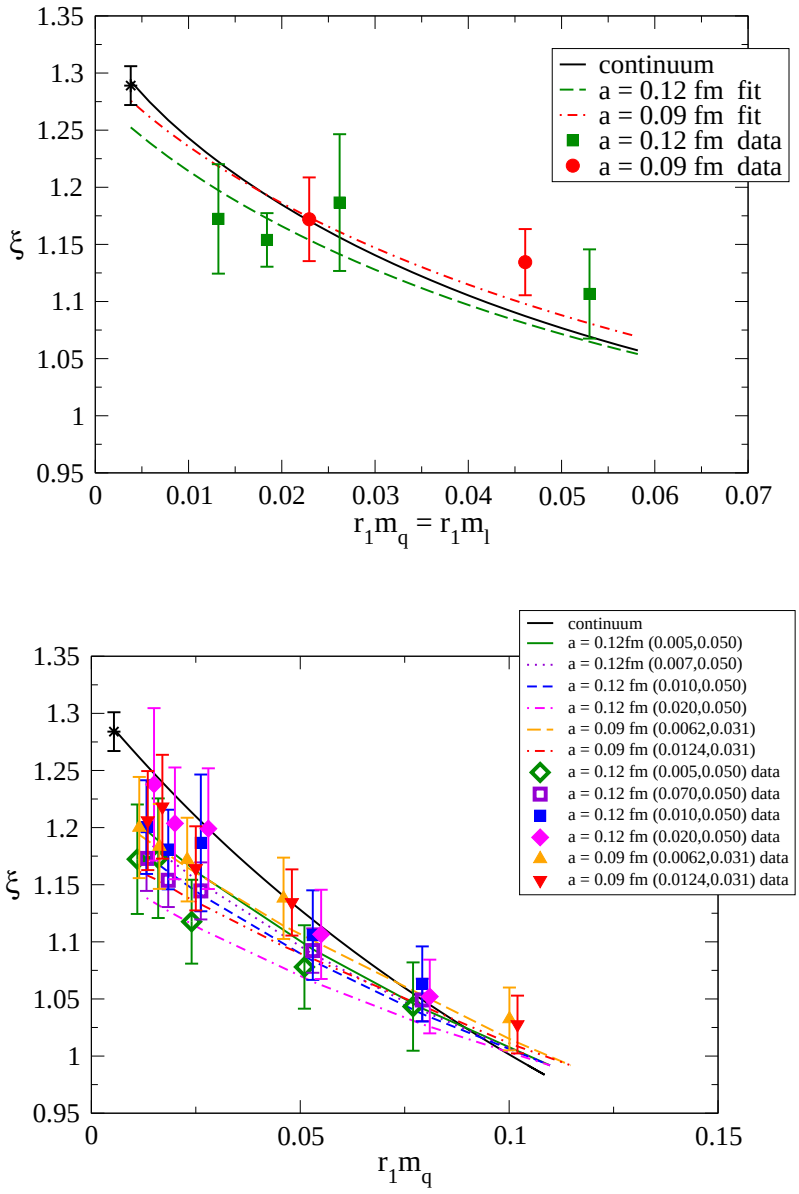

FIG. 5. Fits results using the NLO rHMSχPT, first line in Eq. (5.6). The (black) star is the physical value of ξ in both plots. The top plot shows only the full QCD data, while the bottom one shows all the data included in the fits. The (green) squares and (red) circles and lines in the upper plot represent the 0.12 fm and 0.09 fm data and fit results respectively. In the bottom plot, each color (symbol) labels a different ensemble.

and, as mentioned above, the fact that direct and indirect fits agree better at NNLO, we choose the direct NNLO fit for our central value and statistical error. The systematic error associated with our choice of fit function is discussed in Sec. VI D.

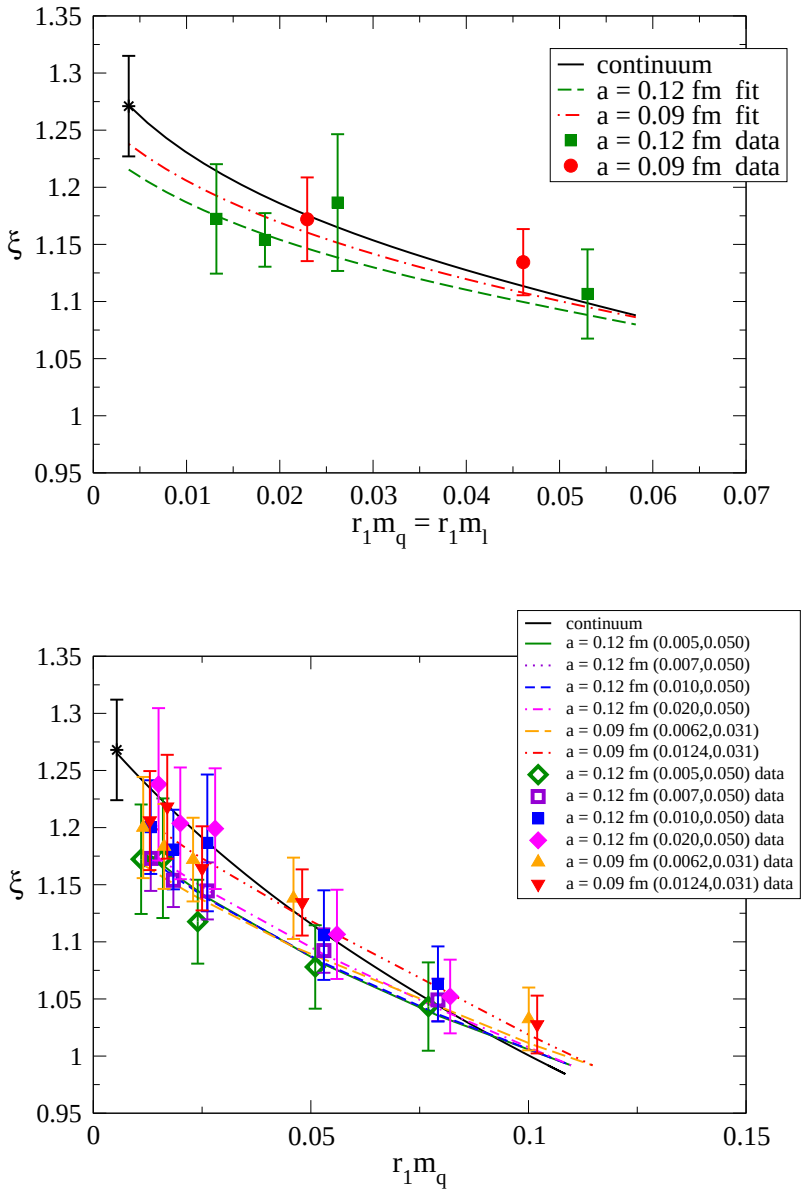

FIG. 6. Fits results using the NNLO rHMSχPT in Eq. (5.6). The (black) star is the physical value of ξ in both plots. The top plot shows only the full QCD data, while the bottom one shows all the data included in the fits. The (green) squares and (red) circles and lines in the upper plot represent the 0.12 fm and 0.09 fm data and fit results, respectively. In the bottom plot, each color (symbol) labels a different ensemble.

VI. ERROR ANALYSIS

In this section, we discuss all sources of systematic uncertainty affecting our calculation of ξ. The systematic errors have to be added to the statistical uncertainty listed in Table V, which also encompasses our imperfect knowledge about chiral parameters such as $g_{B^*B\pi}$ and

$\delta'_{V,A}$.

A. Heavy-quark mass uncertainty

The mixing parameters depend on the b quark mass used in our simulations through the hopping parameter κ_b, which is tuned so that the kinetic meson mass, M_2, agrees with experiment. The dispersion relation for a heavy particle can be written for low-momentum as

$$E(\boldsymbol{p}) = M_1 + \frac{\boldsymbol{p}^2}{2M_2} - \frac{a^3 W_4}{6}\sum_j p_j^4 - \frac{(\boldsymbol{p}^2)^2}{8M_4^3} + O(\boldsymbol{p}^6), \tag{6.1}$$

where κ_b enters into the definitions of M_1 and M_2 [40]. W_4 and the deviation of M_4 from M_2 capture lattice artifacts. We calculated two-point functions for the pseudoscalar and vector mesons at several momenta and extract the energy, $E(\boldsymbol{p})$, for each particle at each momentum. A fit to the dispersion relation then determines M_2 and the spin average of the results is taken. The κ_b value is then adjusted until M_2 agrees with the spin-averaged B_s meson mass.

In this work, we use the values for κ_b on the $a \approx 0.12$ fm and $a \approx 0.09$ fm ensembles tuned this way in Ref. [55]. The error in the determination translates into a systematic error in the mixing matrix elments. However, in the ratio ξ the effect of the uncertainty is minimal, since the corrections go in the same direction in both denominator and numerator, and, thus, largely cancel. In addition, most of the remaining dependence is encoded in the decay constants rather than in the bag parameters, which are very insensitive to the exact values of the quark masses. In Ref. [59], we studied the decay constants with the same choice of actions, parameters, and configurations as here. We expect systematic errors to be very similar in both analyses. We therefore adopt the error due to the uncertainty in the b quark mass obtained in Ref. [59] for the ratio of decay constants f_{B_s}/f_{B_d}, namely, 0.4%, as a good estimate of this systematic error for ξ.

B. Higher-order effects in the perturbative matching

The most straightforward and conservative way to estimate the effects of the missing higher order terms in the perturbative matching is to assume two-loop coefficients of order 1 and to multiply the central value by $\alpha_s^2 = \alpha_V^2(2/a)$. This estimate gives an error $\sim 5\%$ for $f_B\sqrt{B_B}$ on the $a \approx 0.12$ fm lattices and $\sim 3.6\%$ on the $a \approx 0.09$ fm lattices, becoming the main source of uncertainty for this quantity [37]. If there was no mixing between $\langle\mathcal{O}_1\rangle$ and $\langle\mathcal{O}_2\rangle$ under renormalization, there would be an exact cancellation of the renormalization coefficients for the ratio $\xi = (f_{B_s}\sqrt{B_{B_s}})/(f_{B_d}\sqrt{B_{B_d}})$, as long as the valence light-quarks are taken to be massless in the renormalization calculation. The mixing under renormalization prevents this exact cancellation from happening, but the renormalization corrections in the ratio are still largely suppressed, by a factor of $\langle\mathcal{O}_2^s\rangle/\langle\mathcal{O}_1^s\rangle - \langle\mathcal{O}_2^d\rangle/\langle\mathcal{O}_1^d\rangle$, with respect to those for a single matrix element. We estimate this suppression factor via the ratio $(m_s - m_d)/\Lambda_{\rm QCD}$ and multiply the perturbative error for $f_B\sqrt{B_B}$ given above by it. As a result, the perturbative matching uncertainty for ξ from this estimate is 0.2–0.5% (for $\Lambda_{\rm QCD} = 700$ MeV).

The ratio ξ changes by 0.2% when the one-loop renormalization is omitted entirely, supporting our power-counting argument. Another way of estimating $O(\alpha_s^2)$ effects is by varying the scale q^* at which α_V is evaluated. If we change q^* from our central value of $2/a$ to $1/a$ and $3/a$ we find that the extrapolated ξ changes between 0.2–0.4%.

Since the initial estimate yields the largest uncertainty, 0.5%, we take this as the error associated with the missing higher order terms in the perturbative renormalization. Hence, this source of uncertainty is subdominant in our determination of ξ.

C. Mixing with wrong-spin four-fermion operators

As mentioned in Sec. V, there are contributions at NLO in rHMSχPT originating from the mixing of $\langle\mathcal{O}_1\rangle$ with the matrix elements of four-fermion operators of different spin and taste. We have omitted these contributions from our chiral fits, because we discovered these terms after this stage of the analysis was complete. From Figs. 5 and 6, one can see that the effect of the wrong-spin mixing is unlikely to be very large, perhaps being mostly absorbed into the LECs.

We cannot include the effects of the wrong-spin contributions, because they require the matrix elements of $\mathcal{O}_3$, which we have not computed here. Fortunately, however, we have started a more comprehensive analysis of B-$\bar{B}$ mixing on a larger set of higher-statistics ensembles, including $\mathcal{O}_3$. We have added the wrong-spin operators to that analysis and find that their inclusion tends to increase the slope of the continuum extrapolated chiral fit function for $\langle\mathcal{O}_1\rangle$ and, hence, ξ. For example, taking priors and widths similar to those in Table IV, we find a 2% increase in ξ, while for other reasonable choices of the priors the variation is not larger than 3.2%. We add a 3.2% systematic error to account for the missing terms in our chiral extrapolation functions.

D. Chiral-extrapolation systematics and light-quark discretization

The errors due to the choice of fit ansatz and light-quark discretization effects cannot be disentangled, because every fit ansatz necessarily treats the discretization errors differently. So any estimate of the systematic uncertainty associated with the choice of ansatz also accounts for the light-quark discretization errors left over after removing the dominant ones using rHMSχPT.

In Fig. 7, we show the distribution of values for ξ obtained with the NNLO direct fit for the 200 bootstrap samples analyzed. We check that 200 bootstrap samples is enough to obtain a (nearly) Gaussian distribution, as can be seen in the plot. With the goal of testing our choice of functional form and the error associated with the truncation of the chiral series, we perform fits with only two of the three NNLO terms, omitting each one in turn. All fits give good values of χ^2/d.o.f. and p value. The values of ξ obtained are scattered around the distribution in Fig. 7 but always within 1.5 statistical σ of the central value. This consistency, together with the fact that the NNLO LECs are not well determined by the fit, indicates that the statistical error already accounts for the possibility of having one of the unknown constants equal or close to zero. If we inflate and symmetrize our statistical errors to ± 0.047, we cover the spread of results from the different fitting functions tried (including the NLO one). We take this value as our estimate of both statistical and chiral systematic uncertainties.

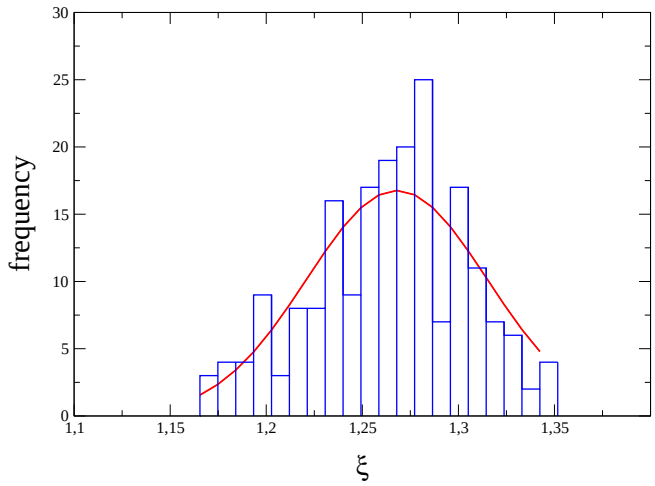

FIG. 7. Histogram of the distribution of values of ξ obtained from the 200 bootstrap samples. The red line is a Gaussian distribution corresponding $\xi = 1.268 \pm 0.047$ (the NNLO result with augmented errors as explained in the text).

TABLE VI. Input for the physical light-quark masses used in the chiral extrapolations. These values were determined by the MILC collaboration [87, 100]. Physical values are found from chiral fits that have been extrapolated to the continuum, but masses are still in units of the $a \approx 0.09$ fm lattice spacing.

Quantity	Physical
$am_s \times 10^2$	2.72 (8)
$a\frac{(m_u+m_d)}{2} \times 10^3$	0.997(35)
$am_d \times 10^3$	1.40(6)

An alternative way of estimating the uncertainty in the truncation of the chiral series and the fitting function would be taking the difference between the NLO and the NNLO fits results. If we add this difference with the statistical errors in Table V in quadrature, the uncertainty would be slightly smaller than the ± 0.047 we are taking as our estimate of these two sources of error.

In the rest of this section, we list the errors associated with the uncertainty of several input parameters used in the continuum and chiral fits, that typically can be estimated by varying the inputs and redoing the fits.

1. Light-quark mass uncertainty

The physical values of the light-quark masses used for the extrapolations and interpolations for ξ are determined by the MILC collaboration [87, 100]. They are obtained by making the charged pions and kaons take on their physical values after removal of electromagnetic effects and are listed in Table VI.

The error on ξ due to the light-quark mass uncertainties is obtained by individually varying each quark mass within this uncertainty and repeating the preferred chiral fit and extrapolation. The central values arrived at using each mass variation are compared to the results of the fit which used the central values for the masses, and their differences are added in quadrature. This gives a total systematic error due to the light-quark mass uncertainties of 0.5% for ξ.

2. Uncertainty in the scale r_1

The value of r_1 used in this analysis to convert from lattice to physical units, as described in Sec. V A, is $r_1 = 0.3117(22)$ fm. The results discussed in previous sections are obtained by fixing r_1 to its central value. In order to estimate the uncertainty due to the error in r_1 we change r_1 by ± 0.0022 fm and all parameters that depend on the physical r_1 are appropriately adjusted. The uncertainty in scale gives a systematic error of 0.2%, which is very small due to the fact that ξ is a dimensionless quantity and the scale only enters in the normalization to lattice units of the chiral corrections $(1/(f_\pi r_1)^2)$ and indirectly via the tuning of the quark masses.

E. Heavy-quark discretization effects

The discretization errors associated with our choice of heavy-quark action to simulate the bottom quarks can be described in terms of the difference in the lattice and continuum Wilson coefficients of higher dimension operators in the HQET expansion. Those come from two sources: the mismatch between continuum and lattice in the Lagrangian and the mismatch in the four-fermion operators whose matrix elements yield $f_B\sqrt{B_B}$ and, thus, ξ. For a particular operator Q_i the error can be written in terms of the usual power counting magnitudes times functions that reflect the particular $m_0 a$ dependence of the action [56, 101]

$$\texttt{error}_i = z_i f_i(m_0 a)\,(a\Lambda_{\rm QCD})^{s_i}\ , \tag{6.2}$$

where $s_i = \dim Q_i - 4$ for Lagrangian operators Q_i of dimension 4 and 5, and $s_i = \dim Q_i - 6$ for four-fermion operators Q_i of dimension 7 and 8, and the z_i are constants. The functions $f_i(m_0 a)$ can be deduced from references [40, 102] and were discussed in detail in [56] for the form factors parametrizing $B \to \pi l \nu$ decays and in [59] for heavy-light decay constants. A detailed study of these corrections for the matrix elements of all the operators contributing to neutral B mixing in the SM and beyond will be presented elsewhere [77]. Here we only summarize the sources of the different corrections for $\langle \mathcal{O}_1 \rangle$ and ξ. The explicit form of the different functions $f_i(m_0 a)$ can be found in Appendix B.

From the Lagrangian, there are $O(a^2)$ errors and $O(\alpha_s a)$ errors which are identical to those in Eqs. (A12) and (A19) in Ref. [59]. They are proportional to the functions $f_E(m_0 a)$ in Eq. (B1) and $f_B(m_0 a)$ in Eq. (B2) of Appendix B, respectively.

From the four-fermion operators, we have $O(a^2)$ errors coming from higher order corrections to the rotation relation Eq. (2.29). They are generated by the mismatch between lattice and continuum coefficients of the operators $\bar{q}\Gamma \boldsymbol{D}^2 b$, $\bar{q}\Gamma i\boldsymbol{\Sigma}\cdot\boldsymbol{B} b$ and $\bar{q}\Gamma\boldsymbol{\alpha}\cdot\boldsymbol{E} b$ in the same way as in Eqs. (A13) and (A14) of Ref. [59], but with an extra overall factor of two due to the fact that we have two heavy fields in our leading-order operator, not one. These corrections are proportional to the functions $f_X(m_0 a)$ and $f_Y(m_0 a)$ in Eq. (B3) of Appendix B,

TABLE VII. Heavy-quark discretization errors given in percent.

Contribution	f_i	z_i	Error $f_B\sqrt{B_B}$ (%) (coarse,fine)	Error ξ (%) (coarse,fine)
$O(a^2)$ Lagrangian	f_E	2	(0.28,0.16)	
$O(\alpha_s a)$ Lagrangian	f_B	2	(0.96,0.58)	
$O(a^2)$ Operator	f_X	4	(1.29,0.74)	
	f_Y	2	(0.23,0.18)	
$O(\alpha_s a)$ Operator	f_3	3	(1.32,0.75)	
Total error			(2.1,1.3)	(0.2,0.1)

respectively.

The last contribution, and the least straightforward, comes from the $O(\alpha_s a)$ corrections to the four-fermion operators. In principle, to subleading order, there are a basis of twelve new local operators in the effective Hamiltonian. However, using symmetry constraints, Fierz transformations and rewriting some combinations as total derivatives, only five independent operators remain [37, 103]. Because we separate the temporal and spatial parts of the operators through this analysis, the total temporal and spatial components of those five operators should be compared with the temporal and spatial parts of the leading operators. As explained in Ref. [77], this produces a difference of $3f_3(m_0 a)$, where f_3 is given in Eq. (B4).

In Table VII, we list all the contributions together with the functions f_i, and the proportionality constant z_i in Eq. (6.2). We also list the numerical values of the different contributions to the heavy-quark discretization error in percentage for $f_B\sqrt{B_B}$. In order to get the numerical results, we use $\Lambda_{\rm QCD} = 700$ MeV and $\alpha_s = \alpha_V(2/a)$ listed in Table II. The final heavy-quark discretization error for $f_B\sqrt{B_B}$ is 1.3% for the $a \approx 0.09$ fm ensembles and 2.1% for the 0.12 fm ones.

These errors largely cancel in ξ. The effect of the cancellation on the error can be estimated by multiplying the errors in $f_B\sqrt{B_B}$ by a factor of $(m_s - m_d)/\Lambda_{\rm QCD}$ which gives a final heavy-quark discretization error for ξ of 0.2% for the coarse lattice and 0.1% for the fine lattice. This agrees well with the estimate of this type of error for the ratio f_{B_s}/f_B [59], $\sim 0.3\%$, using a very similar set of data and statistics. The strategy followed in Ref. [59] differs from the one described here. In that paper, terms of the form in (6.2) were directly added to the chiral and continuum extrapolation fitting functions with a coefficient of order one to be determined by the fit. Ultimately, we would like to employ that strategy also for B^0-$\bar{B}^0$ mixing studies. For this work, however, we simply take the larger estimate from the ratio f_{B_s}/f_B as our estimate of the uncertainty in ξ due to heavy-quark discretization errors.

F. Finite volume corrections

In order to evaluate the finite volume corrections in our calculation, we follow the prescription in Refs. [67] and [104]. The MILC lattices are large enough in the time direction that it can be treated as infinite to a very good approximation, so we are interested in corrections due to finite spatial volume only. They are estimated by replacing infinite-volume integrals in the chiral expression with finite sums over the spatial momentum.

Including finite volume corrections in the chiral expressions and redoing the fits reveals

TABLE VIII. Complete error budget and total error for the B^0 mixing parameter ξ. All errors are given in percent.

Source of uncertainty	Error (%)
Statistics $\oplus$ light-quark disc. $\oplus$ chiral extrapolation	3.7
Mixing with wrong-spin operators	3.2
Heavy-quark discretization	0.3
Scale uncertainty (r_1)	0.2
Light-quark masses	0.5
One-loop matching	0.5
Tuning κ_b	0.4
Finite volume	0.1
Mistuned coarse u_0	0.1
Total Error	5.0

negligible errors, $< 0.1\%$.

G. Tuning of the tadpole parameter u_0

The tadpole improvement factor u_0 is a parameter of the gauge and asqtad staggered (sea) quark action and is determined from the fourth root of the average plaquette. The tadpole improvement factor also enters into the valence light and heavy quark actions. On the $a \approx 0.09$ fm ensembles, the valence quarks are generated with the same values of u_0 as the sea. However, on the $a \approx 0.12$ fm ensembles, the valence quark actions use values of u_0 obtained from the average link in Landau gauge instead. The differences between the values of u_0 obtained with the two methods is around 3-4%.

The effect on f_{B_s}/f_B of the mismatch between u_0 values in the valence and the sea sectors of the $a \approx 0.12$ fm ensembles was estimated to be $< 0.1\%$ in Ref [59]. Since this is much smaller than the errors due to statistics, chiral fits, and continuum and chiral extrapolation, we take this estimate as our error on ξ.

VII. DISCUSSION OF RESULTS AND FUTURE IMPROVEMENTS

The error budget for the $SU(3)$-breaking mixing parameter ξ described in the previous sections is summarized in Table VIII. For the first error in the table we prefer not to attempt to disentangle the statistical, light-quark discretization, and chiral extrapolation errors since, as explained in Sec. VI D, the lack of knowledge about the LECs at NNLO makes a reliable separation impossible. Our final result is

$$\xi = 1.268 \pm 0.063\,. \tag{7.1}$$

The total uncertainty is dominated by the combined statistical, light-quark discretization, and chiral extrapolation error, and the uncertainty associated with the wrong-spin operators in the chiral-continuum extrapolation.

Combining our result in Eq. (7.1) with the averages of the experimentally measured values of the mass differences $\Delta M_d = (0.507 \pm 0.004)$ ps^{-1} [16] and $\Delta M_s = (17.69 \pm 0.08)$ ps^{-1} [105], and the meson masses $M_{B_s^0} = (5366.0 \pm 0.9)$ MeV and $M_{B_d^0} = (5279.5 \pm 0.5)$ MeV [16], we quote a value for the ratio of the CKM matrix elements

$$\left|\frac{V_{td}}{V_{ts}}\right| = 0.216 \pm 0.011\,, \tag{7.2}$$

assuming no new physics in $B^0_{(s)}$-$\bar{B}^0_{(s)}$ mixing. The error includes the uncertainties in the B-meson masses and mass differences but it is strongly dominated by the error in ξ.

We can also take our result for ξ and combine it with the value of the decay constant ratio $f_{B_s}/f_{B_d} = 1.229 \pm 0.026$ calculated by our collaboration [59] to determine the ratio of bag parameters

$$\frac{B_{B_s}}{B_{B_d}} = \xi^2 \left(\frac{f_{B_d}}{f_{B_s}}\right)^2 = 1.06 \pm 0.11\,. \tag{7.3}$$

The two results for ξ and f_{B_s}/f_{B_d} are correlated, but the statistical analyses were done indepedently so we cannot include the correlations in calculating the uncertainty in the ratio of bag parameters. Therefore the error shown in the result of Eq. (7.3) is overestimated. However, as part of the future work, we plan to perform a common analysis of matrix elements and decay constants, from which we will be able to account for correlations in extracting the value of the bag parameters and thus greatly reduce the error in (7.3). We will do the same for the individual bag parameters corresponding to all the operators in the basis in (1.3).

Our result for ξ in Eq. (7.1) is in good agreement with the HPQCD value obtained in Ref. [32], $\xi = 1.258(33)$. Note, however, that HPQCD did not estimate the effects of the wrong-spin operators that appear in the complete NLO chiral expression, so the full error in their result may be somewhat bigger than what was quoted. The agreement of these two determinations of ξ provides an excellent check of the methodology and systematic error study in both analyses. In addition, it helps to increase the confidence in the robustness of lattice results for a parameter of great importance in phenomenological studies. In this article, we have established and tested the methodology to apply to broader studies of B^0 mixing with the same lattice formulations for light and bottom quarks as used here.

Statistical errors could be reduced significantly by expanding the analysis to include the full set of available configurations (approximately 2000) at each of the $a \approx 0.12$ fm and $a \approx 0.09$ fm ensembles. The current runs of our collaboration on the extended ensembles are also implementing sources located at a random spatial and time location to reduce further the statistical errors. We expect a reduction of the statistical errors by about a factor of two.

The other dominant error of our calculation, the omission in the rHMSχPT analysis of terms generated by wrong-spin operators, will be eliminated when a complete analysis is done with the full rHMSχPT expressions [86]. A result for ξ that properly includes the wrong-spin terms requires the calculation of the continuum matrix elements not only of the operator $\mathcal{O}_1$ as we have done in this work, but also of $\mathcal{O}_2$ and $\mathcal{O}_3$, and simultaneous chiral and continuum extrapolations of all three matrix elements.

The discretization errors, related to both heavy and light quarks, will be reduced in a straightforward way by simulations at smaller lattice spacing, *i.e.*, on the $a \approx 0.06$ fm and

$a \approx 0.045$ fm MILC lattices. The reduction of both statistical and discretization errors will also yield cleaner and more accurate continuum and chiral extrapolations. Including data at smaller lattice spacings will also reduce the uncertainty associated with the perturbative matching from the reduction of $\alpha_s = \alpha_V(2/a)$. Although not relevant for the reduction of the total error in ξ, this will be important in the determination of the matrix elements $\langle \mathcal{O}_i \rangle$ themselves.

Similarly, although the uncertainty associated with heavy-quark discretization effects is a subdominant source of error in the determination of ξ, it is one of the main errors in the determination of $\langle \mathcal{O}_i \rangle$ [37]. In order to have a more reliable, data-driven estimation of these effects, in our on-going analyses we plan to employ the strategy used in Ref. [59], in which terms like the ones in (6.2) are included in the chiral-continuum extrapolation fitting form with free parameters to be determined from the fit.

Our new analysis, which incorporates the improvements mentioned above, includes the study of the matrix elements of all five operators that contribute to $H_{eff}^{\Delta B=2}$ [29]. This will allow not only the precise SM determination of $\Delta M_{s,d}$, $\Delta\Gamma_{s,d}$, and ξ, but will also provide the nonperturbative inputs needed to put constraints on BSM models using experimental data on B^0 mixing and related observables.

ACKNOWLEDGMENTS

Computations for this work were carried out with resources provided by the USQCD Collaboration, the Argonne Leadership Computing Facility, the National Energy Research Scientific Computing Center, and the Los Alamos National Laboratory, which are funded by the Office of Science of the U.S. Department of Energy; and with resources provided by the National Institute for Computational Science, the Pittsburgh Supercomputer Center, the San Diego Supercomputer Center, and the Texas Advanced Computing Center, which are funded through the National Science Foundation's Teragrid/XSEDE Program. This work was supported in part by the U.S. Department of Energy under Grants No. DE-FC02-06ER41446 (C.D., L.L., M.B.O.), No. DE-FG02-91ER40661 (S.G.), No. DE-FG02-91ER40677 (C.M.B, R.T.E., E.D.F., E.G., R.J., A.X.K.), No. DE-FG02-91ER40628 (C.B.), No. DE-FG02-04ER-41298 (D.T.); by the National Science Foundation under Grants No. PHY-0555243, No. PHY-0757333, No. PHY-0703296, No. PHY10-67881 (C.D., L.L., M.B.O.), No. PHY-0757035 (R.S.), and No. PHY-0704171 (J.E.H.); by the MICINN, Spain, under grant FPA2010-16696 and *Ramón y Cajal* program (E.G.); by Junta de Andalucía, Spain, under grants FQM-101, FQM-330, FQM-03048, and FQM-6552 (E.G.); by the URA Visiting Scholars' program (C.M.B., R.T.E., E.G., M.B.O.); by the Fermilab Fellowship in Theoretical Physics (C.M.B.); and by the Science and Technology Facilities Council and the Scottish Universities Physics Alliance (J.L.). This manuscript has been co-authored by employees of Brookhaven Science Associates, LLC, under Contract No. DE-AC02-98CH10886 with the U.S. Department of Energy. Fermilab is operated by Fermi Research Alliance, LLC, under Contract No. DE-AC02-07CH11359 with the United States Department of Energy.

Appendix A: Staggered Chiral Perturbation Theory for B^0-$\bar{B}^0$ mixing

In this appendix we describe the functional form we use in the chiral and continuum extrapolation of the matrix elements $\langle \overline{B}_q^0 | \mathcal{O}_1^q | B_q^0 \rangle$. Further discussion, as well as complete

NLO rHMSχPT expressions for $\langle \overline{B}_q^0 | \mathcal{O}_i^q | B_q^0 \rangle$ with $i = 1, \ldots, 5$ and the corresponding bag parameters can be found in [86].

At NLO in rHMSχPT and at first order in the heavy-quark expansion we use

$$\langle \overline{B}_q^0 | \mathcal{O}_1^q | B_q^0 \rangle = \alpha \left(1 + \frac{\mathcal{W}_{q\bar{b}} + \mathcal{W}_{b\bar{q}}}{2} + \mathcal{T}_q + \mathcal{Q}_q \right) + L_v m_q + L_s (2m_l + m_h) + L_a a^2 \,. \tag{A1}$$

α, L_v, L_s, and L_a are constants to be determined from the fits to lattice data. The quantities in script for the partially quenched 2+1 ($m_u = m_d \neq m_s$) case are

$$\begin{aligned} \mathcal{W}_{q\bar{b}} = \mathcal{W}_{b\bar{q}} = \frac{i g^2_{B^* B\pi}}{f_\pi^2} \Bigg\{ & \frac{1}{16} \sum_{\mathcal{S},\rho} N_\rho \, \mathcal{H}^{\Delta^* + \delta_{\mathcal{S}q}}_{q\mathcal{S},\rho} + \frac{1}{3} \Bigg[R^{[2,2]}_{X_I}\big(\{M^{(5)}_{X_I}\};\{\mu_I\}\big) \, \frac{\partial \mathcal{H}^{\Delta^*}_{X,I}}{\partial m^2_{X_I}} \\ & - \sum_{j \in \{M^{(5)}_I\}} D^{[2,2]}_{j,X_I}\big(\{M^{(5)}_{X_I}\};\{\mu_I\}\big) \mathcal{H}^{\Delta^*}_{j,I} \Bigg] + a^2 \delta'_V \Bigg[R^{[3,2]}_{X_V}\big(\{M^{(7)}_{X_V}\};\{\mu_V\}\big) \, \frac{\partial \mathcal{H}^{\Delta^*}_{X,V}}{\partial m^2_{X_V}} \\ & - \sum_{j \in \{M^{(7)}_V\}} D^{[3,2]}_{j,X_V}\big(\{M^{(7)}_{X_V}\};\{\mu_V\}\big) \mathcal{H}^{\Delta^*}_{j,V} \Bigg] + \big(V \to A\big) \Bigg\}. \end{aligned} \tag{A2}$$

$$\begin{aligned} \mathcal{T}_q = \frac{-i}{f_\pi^2} \Bigg\{ & \frac{1}{16} \sum_{\mathcal{S},\rho} N_\rho \, \mathcal{I}_{q\mathcal{S},\rho} + \frac{1}{16} \sum_{\rho} N_\rho \mathcal{I}_{X,\rho} + \frac{2}{3} \Bigg[R^{[2,2]}_{X_I}\big(\{M^{(5)}_{X_I}\};\{\mu_I\}\big) \left(\frac{\partial \mathcal{I}_{X_I}}{\partial m^2_{X_I}} \right) \\ & - \sum_{j \in \{M^{(5)}_I\}} D^{[2,2]}_{j,X_I}\big(\{M^{(5)}_{X_I}\};\{\mu_I\}\big) \mathcal{I}_j \Bigg] + a^2 \delta'_V \Bigg[R^{[3,2]}_{X_V}\big(\{M^{(7)}_{X_V}\};\{\mu_V\}\big) \left(\frac{\partial \mathcal{I}_{X_V}}{\partial m^2_{X_V}} \right) \\ & - \sum_{j \in \{M^{(7)}_V\}} D^{[3,2]}_{j,X_V}\big(\{M^{(7)}_{X_V}\};\{\mu_V\}\big) \mathcal{I}_j \Bigg] + \big(V \to A\big) \Bigg\}, \end{aligned} \tag{A3}$$

$$\begin{aligned} \mathcal{Q}_q = \frac{-i g^2_{B^* B\pi}}{f_\pi^2} \Bigg\{ & \frac{1}{16} \sum_{\rho} N_\rho \mathcal{H}^{\Delta^*}_{X,\rho} + \frac{1}{3} \Bigg[R^{[2,2]}_{X_I}\big(\{M^{(5)}_{X_I}\};\{\mu_I\}\big) \left(\frac{\partial \mathcal{H}^{\Delta}_{X_I}}{\partial m^2_{X_I}} \right) \\ & - \sum_{j \in \{M^{(5)}_I\}} D^{[2,2]}_{j,X_I}\big(\{M^{(5)}_{X_I}\};\{\mu_I\}\big) \mathcal{H}^{\Delta}_{j} \Bigg] \Bigg\}, \end{aligned} \tag{A4}$$

In the equations above, the index ρ runs over the taste representation (P, A, T, V, I) with degeneracies N_ρ (N_ρ =1,4,6,4,1, respectively), and $\mathcal{S}$ runs over the sea flavors u, d, s. The meson X is made of two light valence quarks q, and m_X is its mass. The functions $\mathcal{H}$ and $\mathcal{I}$ are the integrals defined in Appendix A of [85]. The subscripts on those functions label the flavor and taste of the meson masses at which they are evaluated.

The superscript in $\mathcal{H}$ is the second argument for that function as defined in [85]. In

addition to the hyperfine splitting $\Delta^* = M_{B^*} - M_B$, it includes a light flavor splitting $\delta_{\mathcal{S}q}$ whenever the light flavor of the vector meson in the loop is different from the external flavor.

The splitting is $\delta_{\mathcal{S}q} \equiv M_{B_{\mathcal{S}}^0} - M_{B_q^0} = 2\lambda_1\mu(m_{\mathcal{S}} - m_q)$, where λ_1 and μ are low energy constants. The constant λ_1 comes from heavy quark effective theory, and μ is defined in (5.2).

The residues functions $R_j^{[n,k]}$ and $D_{j,l}^{[n,k]}$ in the expressions above are defined by [65]

$$\begin{aligned} R_j^{[n,k]}(\{m\},\{\mu\}) &\equiv \frac{\prod_{a=1}^{k}(\mu_a^2 - m_j^2)}{\prod_{i\neq j}(m_i^2 - m_j^2)}, \\ D_{j,l}^{[n,k]}(\{m\},\{\mu\}) &\equiv -\frac{d}{dm_l^2} R_j^{[n,k]}(\{m\},\{\mu\}). \end{aligned} \tag{A5}$$

The mass combinations appearing as arguments of these functions in the 2+1 partially quenched theory are

$$\begin{aligned} \{M_X^{(5)}\} &\equiv \{m_\eta, m_X\}, \\ \{M_X^{(7)}\} &\equiv \{m_\eta, m_{\eta'}, m_X\}, \\ \{\mu\} &\equiv \{m_L, m_H\}, \end{aligned} \tag{A6}$$

where m_L is the meson mass made from $l\bar{l}$ sea quarks, and m_H is the meson mass made from $h\bar{h}$ sea quarks. The tastes of these mesons are indicated explicitly in the equations above.

Since we are not including the effects of the hyperfine splitting Δ^* or the light flavor splittings δ_k in this work, the functions $\mathcal{H}$ and $\mathcal{I}$ appearing in the wave function, tadpole, and sunset contributions simplify to

$$i\mathcal{H}_{k,\Xi}^0 = -3i\mathcal{I}_{k,\Xi} = -\frac{3}{16\pi^2} M_{k,\Xi}^2 \ln\left(\frac{M_{k,\Xi}^2}{\Lambda_\chi^2}\right). \tag{A7}$$

Appendix B: Functions parametrizing heavy-quark discretization errors

In this Appendix we collect the functions f_i needed in Eq. (6.2) to estimate the heavy-quark discretization errors affecting our calculation. For details on the origin of these functions and the effects of higher-dimension operators in the lagrangian, see [102]. For further details on the application to the estimation of heavy-quark discretization errors in $B^0 - \bar{B}^0$ mixing, see [77].

- $O(a^2)$ errors from the Lagrangian.

$$f_E(m_0 a) = \frac{1}{2}\left[\frac{(1+m_0 a)-1}{m_0 a(2+m_0 a)(1+m_0 a)} - \frac{1}{4(1+m_0 a)^2}\right] \tag{B1}$$

- $O(\alpha_s a^2)$ errors from the Lagrangian

$$f_B(m_0 a) = \frac{\alpha_s}{2(1+m_0 a)} \tag{B2}$$

- $O(a^2)$ errors from the four-fermion operator

$$f_X(m_0a) = \frac{1}{2}\left[\frac{1}{2(1+m_0a)} - \left(\frac{m_0a}{2(2+m_0a)(1+m_0a)}\right)^2\right]$$
$$f_Y(m_0a) = \frac{2+4m_0a+(m_0a)^2}{4(1+m_0a)^2(2+m_0a)^2} \tag{B3}$$

- $O(\alpha_s a^2)$ errors from the four-fermion operator

$$f_3(m_0a) = \frac{\alpha_s}{2(2+m_0a)} \tag{B4}$$

Appendix C: Prior central values and widths for the correlator fits

In the table below we collect the prior central values and widths used in the correlator fits described in Sec. IV. The amplitude parameters are defined in Eqs. (2.21) and (2.22), and the energy differences are defined as $\Delta E_{i+1,i} \equiv a(E_{i+1} - E_1)$.

TABLE IX. The priors with index 0 refer to the ground state. Superscripts d and $1S$ refer to the local and 1S smeared sources respectively. Higher energy state priors have indices i and j. The prime in E_i' refers to an opposite parity (oscillating) state.

	Prior central value	Prior width
Z_0^{1S}	2.2	0.5
Z_i^{1S}	0.01	0.5
Z_0^d	0.45	0.45
Z_i^d	0.01	1
O_{00}	0.01	0.02
O_{ij}	0.01	0.1
E_0 (0.12 fm)	1.95	0.15
E_0' (0.12 fm)	2.25	0.15
E_0 (0.09 fm)	1.65	0.15
E_0' (0.09 fm)	1.85	0.15
$\log \Delta E_{i+1,i}$	-1.5	0.5
$\log \Delta E'_{i+1,i}$	-1.5	0.5

[1] E. Lunghi and A. Soni, Phys. Lett. B **697**, 323 (2011) [arXiv:1010.6069 [hep-ph]].
[2] V. M. Abazov *et al.* [DØ], Phys. Rev. Lett. **105** (2010) 081801. [arXiv:1007.0395 [hep-ex]].
[3] J. Laiho, E. Lunghi, R. Van De Water, PoS **FPCP2010** (2010) 040 [arXiv:1102.3917 [hep-ph]];
[4] A. Lenz *et al.*, arXiv:1203.0238 [hep-ph].

[5] E. Lunghi and A. Soni, Phys. Rev. Lett. **104** (2010) 251802 [arXiv:0912.0002 [hep-ph]];
[6] A. Lenz *et al.*, Phys. Rev. D **83** (2011) 036004; [arXiv:1008.1593 [hep-ph]];
[7] A. J. Bevan *et al.* [UTfit], PoS **ICHEP2010**, 270 (2010) [arXiv:1010.5089 [hep-ph]].
[8] A. Lenz and U. Nierste, JHEP **0706** (2007) 072 [arXiv:hep-ph/0612167].
[9] M. Bona *et al.* [UTfit], PMC Phys. A **3**, 6 (2009) [arXiv:0803.0659 [hep-ph]].
[10] T. Aaltonen *et al.* [CDF], arXiv:1112.1726 [hep-ex];
[11] V. M. Abazov *et al.* [D0],
Phys. Rev. D **85** (2012) 032006 [arXiv:1109.3166 [hep-ex]];
[12] K. Anikeev *et al., B physics at the Tevatron: Run II and beyond,* arXiv:hep-ph/0201071, Chapters 1.3 and 8.3.
[13] A. Abulencia *et al.* [CDF], Phys. Rev. Lett. **97** (2006) 242003 [arXiv:hep-ex/0609040];
[14] V. M. Abazov *et al.* [DØ], Phys. Rev. Lett. **97** (2006) 021802 [arXiv:hep-ex/0603029].
[15] R. Aaij *et al.* [LHCb], Phys. Lett. B **709**, 177 (2012) [arXiv:1112.4311 [hep-ex]].
[16] K. Nakamura *et al.* [Particle Data Group], J. Phys. G **G37**, 075021 (2010).
[17] M. Bona *et al.* [UTfit], JHEP **0803**, 049 (2008) [arXiv:0707.0636 [hep-ph]].
[18] B. A. Dobrescu and G. Z. Krnjaic, arXiv:1104.2893 [hep-ph].
[19] W. Altmannshofer and M. Carena, arXiv:1110.0843 [hep-ph].
[20] A. J. Buras and J. Girrbach, JHEP **1203**, 052 (2012) [arXiv:1201.1302 [hep-ph]].
[21] M. Blanke, A. J. Buras, K. Gemmler and T. Heidsieck, JHEP **1230**, 024 (2012) [arXiv:1111.5014 [hep-ph]].
[22] A. J. Buras, M. Nagai and P. Paradisi, JHEP **1105**, 005 (2011) [arXiv:1011.4853 [hep-ph]].
[23] A. J. Buras, K. Gemmler and G. Isidori, Nucl. Phys. B **843**, 107 (2011) [arXiv:1007.1993 [hep-ph]].
[24] A. J. Buras, B. Duling, T. Feldmann, T. Heidsieck, C. Promberger and S. Recksiegel, JHEP **1009**, 106 (2010) [arXiv:1002.2126 [hep-ph]].
[25] L. Wolfenstein, Phys. Rev. Lett. **51**, 1945 (1983).
[26] A. J. Buras, M. E. Lautenbacher and G. Ostermaier, Phys. Rev. D **50**, 3433 (1994) [hep-ph/9403384].
[27] F. Gabbiani, E. Gabrielli, A. Masiero and L. Silvestrini, Nucl. Phys. B **477**, 321 (1996) [hep-ph/9604387];
[28] D. Becirevic, V. Gimenez, G. Martinelli, M. Papinutto and J. Reyes, JHEP **0204**, 025 (2002) [hep-lat/0110091].
[29] C. M. Bouchard *et al.* [Fermilab Lattice and MILC], PoS **LATTICE2011**, 274 (2011) [arXiv:1112.5642 [hep-lat]].
[30] T. Inami and C. S. Lim, Prog. Theor. Phys. **65**, 297 (1981) [Erratum-ibid. **65**, 1772 (1981)].
[31] A. J. Buras, M. Jamin and P. H. Weisz, Nucl. Phys. B **347** (1990) 491.
[32] E. Gámiz *et al.* [HPQCD], Phys. Rev. D **80**, 014503 (2009) [arXiv:0902.1815 [hep-lat]].
[33] [RBC and UKQCD] C. Albertus *et al.*, Phys. Rev. **D82**, 014505 (2010) [arXiv:1001.2023 [hep-lat]].
[34] R.T. Evans, A.X. El-Khadra and M. Di Pierro [Fermilab Lattice and MILC], PoS **LAT2006** (2006) 081.
[35] R. Evans, E. Gámiz, A. X. El-Khadra, M. Di Pierro [Fermilab Lattice and MILC], PoS **LAT2007**, 354 (2007). [arXiv:0710.2880 [hep-lat]].
[36] R.T. Evans *et al.* [Fermilab Lattice and MILC], PoS **LAT2008** 052 (2008).
[37] R. T. Evans *et al.* [Fermilab Lattice and MILC], PoS **LAT2009** (2009) 245. [arXiv:0911.5432 [hep-lat]].

[38] G. P. Lepage, L. Magnea, C. Nakhleh, U. Magnea and K. Hornbostel, Phys. Rev. D **46**, 4052 (1992) [hep-lat/9205007].
[39] B. Sheikholeslami and R. Wohlert, Nucl. Phys. B **259**, 572 (1985).
[40] A. X. El-Khadra, A. S. Kronfeld and P. B. Mackenzie, Phys. Rev. D **55** (1997) 3933 [arXiv:hep-lat/9604004].
[41] E. Golowich, J. Hewett, S. Pakvasa and A. A. Petrov, Phys. Rev. D **76**, 095009 (2007) [arXiv:0705.3650 [hep-ph]].
[42] C. W. Bernard *et al.* [MILC], Phys. Rev. D **64**, 054506 (2001) [arXiv:hep-lat/0104002].
[43] M. G. Alford, W. Dimm, G. P. Lepage, G. Hockney and P. B. Mackenzie, Phys. Lett. B **361**, 87 (1995) [arXiv:hep-lat/9507010].
[44] M. Luscher and P. Weisz, Phys. Lett. B **158**, 250 (1985).
[45] S. Prelovsek, Phys. Rev. D **73**, 014506 (2006) [hep-lat/0510080].
[46] C. Bernard, M. Golterman and Y. Shamir, Phys. Rev. D **73**, 114511 (2006) [hep-lat/0604017].
[47] C. Bernard, Phys. Rev. D **73**, 114503 (2006) [hep-lat/0603011].
[48] Y. Shamir, Phys. Rev. D **71**, 034509 (2005) [hep-lat/0412014].
[49] Y. Shamir, Phys. Rev. D **75**, 054503 (2007) [hep-lat/0607007].
[50] C. Bernard, M. Golterman and Y. Shamir, Phys. Rev. D **77**, 074505 (2008) [arXiv:0712.2560 [hep-lat]].
[51] S. R. Sharpe, PoS **LAT2006**, 022 (2006) [hep-lat/0610094].
[52] A. S. Kronfeld, PoS **LAT2007**, 016 (2007) [arXiv:0711.0699 [hep-lat]].
[53] M. Golterman, PoS **CONFINEMENT8**, 014 (2008) [arXiv:0812.3110 [hep-ph]].
[54] G. C. Donald, C. T. H. Davies, E. Follana and A. S. Kronfeld, Phys. Rev. D **84**, 054504 (2011) [arXiv:1106.2412 [hep-lat]].
[55] C. Bernard *et al.* [Fermilab Lattice and MILC], Phys. Rev. D **83**, 034503 (2011) [arXiv:1003.1937 [hep-lat]].
[56] J. A. Bailey *et al.* [Fermilab Lattice and MILC], Phys. Rev. D **79**, 054507 (2009) [arXiv:0811.3640 [hep-lat]].
[57] C. Bernard *et al.* [Fermilab Lattice and MILC], [Phys. Rev. D **79**, 014506 (2009)] [arXiv:0808.2519 [hep-lat]];
[58] J. A. Bailey *et al.* [Fermilab Lattice and MILC], PoS **LATTICE2010**, 311 (2010) [arXiv:1011.2166 [hep-lat]].
[59] A. Bazavov *et al.* [Fermilab Lattice and MILC], arXiv:1112.3051 [hep-lat].
[60] J. A. Bailey *et al.* [Fermilab Lattice and MILC], arXiv:1202.6346 [hep-lat].
[61] C. R. Allton, hep-lat/9610016.
[62] A. Bazavov *et al.* [MILC], Rev. Mod. Phys. **82** (2010) 1349-1417. [arXiv:0903.3598 [hep-lat]].
[63] W. Lee and S. Sharpe, Phys. Rev. D **60**, 114503 (1999) [hep-lat/9905023].
[64] C. Aubin and C. Bernard, Phys. Rev. D **68**, 034014 (2003) [hep-lat/0304014].
[65] C. Aubin and C. Bernard, Phys. Rev. D **68**, 074011 (2003) [hep-lat/0306026].
[66] S. R. Sharpe and R. S. Van de Water, Phys. Rev. D **71**, 114505 (2005) [hep-lat/0409018].
[67] C. Aubin and C. Bernard, Phys. Rev. D **73**, 014515 (2006) [arXiv:hep-lat/0510088].
[68] G. P. Lepage, Phys. Rev. D **59**, 074502 (1999) [arXiv:hep-lat/9809157].
[69] K. Symanzik, Nucl. Phys. B **226**, 205 (1983).
[70] G. P. Lepage and P. B. Mackenzie, Phys. Rev. D **48**, 2250 (1993) [arXiv:hep-lat/9209022].
[71] Z. Hao, G. M. von Hippel, R. R. Horgan, Q. J. Mason and H. D. Trottier, Phys. Rev. D **76**, 034507 (2007) [arXiv:0705.4660 [hep-lat]].

[72] M. Wingate, J. Shigemitsu, C. T. H. Davies, G. P. Lepage and H. D. Trottier, Phys. Rev. D **67**, 054505 (2003) [arXiv:hep-lat/0211014].
[73] L. Susskind, Phys. Rev. D **16**, 3031 (1977); H. S. Sharatchandra, H. J. Thun and P. Weisz, Nucl. Phys. B **192** (1981) 205.
[74] A. S. Kronfeld, Phys. Rev. D **62**, 014505 (2000) [hep-lat/0002008].
[75] G. P. Lepage and P. B. Mackenzie, Phys. Rev. D **48**, 2250 (1993) [hep-lat/9209022].
[76] E. Gámiz, J. Shigemitsu and H. Trottier, Phys. Rev. D **77**, 114505 (2008) [arXiv:0804.1557 [hep-lat]].
[77] E. Gámiz, A. El-Khadra and A. Kronfeld, in preparation.
[78] Q. Mason *et al.* [HPQCD and UKQCD], Phys. Rev. Lett. **95**, 052002 (2005) [hep-lat/0503005].
[79] S. J. Brodsky, G. P. Lepage and P. B. Mackenzie, Phys. Rev. D **28**, 228 (1983).
[80] K. Hornbostel, G. P. Lepage and C. Morningstar, Phys. Rev. D **67**, 034023 (2003) [hep-ph/0208224].
[81] J. L. Richardson, Phys. Lett. B **82**, 272 (1979).
[82] M. Di Pierro *et al.* Nucl. Phys. Proc. Suppl. **119**, 586 (2003) [hep-lat/0210051].
[83] G. P. Lepage *et al.*, Nucl. Phys. Proc. Suppl. **106**, 12 (2002) [arXiv:hep-lat/0110175].
[84] C. Morningstar, Nucl. Phys. Proc. Suppl. **109A**, 185 (2002) [hep-lat/0112023].
[85] W. Detmold and C. J. D. Lin, Phys. Rev. D **76**, 014501 (2007) [arXiv:hep-lat/0612028].
[86] C. Bernard, in preparation.
[87] C. Aubin *et al.* [MILC], Phys. Rev. D **70**, 114501 (2004) [arXiv:hep-lat/0407028].
[88] C. W. Bernard Phys. Rev. D **62**, 034503 (2000) [hep-lat/0002028];
[89] R. Sommer, Nucl. Phys. B **411**, 839 (1994) [hep-lat/9310022].
[90] A. Bazavov *et al.* [MILC], PoS **CD09**, 007 (2009) [arXiv:0910.2966 [hep-ph]].
[91] C. T. H. Davies *et al.* [HPQCD], Phys. Rev. **D81**, 034506 (2010). [arXiv:0910.1229 [hep-lat]].
[92] I. W. Stewart, Nucl. Phys. B **529**, 62 (1998) [arXiv:hep-ph/9803227].
[93] R. Casalbuoni, A. Deandrea, N. Di Bartolomeo, R. Gatto, F. Feruglio, G. Nardulli, Phys. Rept. **281**, 145-238 (1997). [arXiv:hep-ph/9605342 [hep-ph]].
[94] A. Anastassov *et al.* [CLEO], Phys. Rev. **D65**, 032003 (2002). [hep-ex/0108043].
[95] A. Abada, D. Becirevic, P. Boucaud, G. Herdoiza, J. P. Leroy, A. Le Yaouanc, O. Pene, J. Rodriguez-Quintero, Nucl. Phys. Proc. Suppl. **119**, 641-643 (2003) [hep-lat/0209092].
[96] M. C. Arnesen, B. Grinstein, I. Z. Rothstein, I. W. Stewart, Phys. Rev. Lett. **95**, 071802 (2005) [hep-ph/0504209].
[97] H. Ohki, H. Matsufuru, T. Onogi, Phys. Rev. **D77**, 094509 (2008) [arXiv:0802.1563 [hep-lat]].
[98] J. Bulava *et al.* [ALPHA], PoS **LATTICE2010**, 303 (2010). [arXiv:1011.4393 [hep-lat]].
[99] W. Detmold, C. -J. D. Lin and S. Meinel, arXiv:1203.3378 [hep-lat].
[100] C. Bernard PoS **LAT2007**, 090 (2007). [arXiv:0710.1118 [hep-lat]].
[101] A. S. Kronfeld, Nucl. Phys. Proc. Suppl. **129**, 46 (2004) [arXiv:hep-lat/0310063].
[102] M. B. Oktay and A. S. Kronfeld, Phys. Rev. D **78**, 014504 (2008) [arXiv:0803.0523 [hep-lat]].
[103] W. Kilian and T. Mannel, Phys. Lett. B **301**, 382 (1993) [arXiv:hep-ph/9211333].
[104] C. Bernard [MILC], Phys. Rev. D **65**, 054031 (2002) [arXiv:hep-lat/0111051].
[105] Average of the CDF and LHCb results by the Heavy Flavor Averaging Group http://www.slac.stanford.edu/xorg/hfag/